

University of Windsor

Scholarship at UWindor

Electronic Theses and Dissertations

Theses, Dissertations, and Major Papers

1976

A preliminary study of the effect of vibrationally excited hydrogen on oxygen atoms and Excitation of hydrogen fluorescence through near resonant energy transfer from argon.

Richard N. Dubinsky
University of Windsor

Follow this and additional works at: <https://scholar.uwindsor.ca/etd>

Recommended Citation

Dubinsky, Richard N., "A preliminary study of the effect of vibrationally excited hydrogen on oxygen atoms and Excitation of hydrogen fluorescence through near resonant energy transfer from argon." (1976).

Electronic Theses and Dissertations. 709.

<https://scholar.uwindsor.ca/etd/709>

This online database contains the full-text of PhD dissertations and Masters' theses of University of Windsor students from 1954 forward. These documents are made available for personal study and research purposes only, in accordance with the Canadian Copyright Act and the Creative Commons license—CC BY-NC-ND (Attribution, Non-Commercial, No Derivative Works). Under this license, works must always be attributed to the copyright holder (original author), cannot be used for any commercial purposes, and may not be altered. Any other use would require the permission of the copyright holder. Students may inquire about withdrawing their dissertation and/or thesis from this database. For additional inquiries, please contact the repository administrator via email (scholarship@uwindsor.ca) or by telephone at 519-253-3000ext. 3208.



National Library of Canada

Cataloguing Branch
Canadian Theses Division

Ottawa, Canada
K1A 0N4

Bibliothèque nationale du Canada

Direction du catalogage
Division des thèses canadiennes

NOTICE

The quality of this microfiche is heavily dependent upon the quality of the original thesis submitted for microfilming. Every effort has been made to ensure the highest quality of reproduction possible.

If pages are missing, contact the university which granted the degree.

Some pages may have indistinct print especially if the original pages were typed with a poor typewriter ribbon or if the university sent us a poor photocopy.

Previously copyrighted materials (journal articles, published tests, etc.) are not filmed.

Reproduction in full or in part of this film is governed by the Canadian Copyright Act, R.S.C. 1970, c. C-30. Please read the authorization forms which accompany this thesis.

**THIS DISSERTATION
HAS BEEN MICROFILMED
EXACTLY AS RECEIVED**

AVIS

La qualité de cette microfiche dépend grandement de la qualité de la thèse soumise au microfilmage. Nous avons tout fait pour assurer une qualité supérieure de reproduction.

S'il manque des pages, veuillez communiquer avec l'université qui a conféré le grade.

La qualité d'impression de certaines pages peut laisser à désirer, surtout si les pages originales ont été dactylographiées à l'aide d'un ruban usé ou si l'université nous a fait parvenir une photocopie de mauvaise qualité.

Les documents qui font déjà l'objet d'un droit d'auteur (articles de revue, examens publiés, etc.) ne sont pas microfilmés.

La reproduction, même partielle, de ce microfilm est soumise à la Loi canadienne sur le droit d'auteur, SRC 1970, c. C-30. Veuillez prendre connaissance des formules d'autorisation qui accompagnent cette thèse.

**LA THÈSE A ÉTÉ
MICROFILMÉE TELLE QUE
NOUS L'AVONS REÇUE**

A PRELIMINARY STUDY
OF THE EFFECT
OF VIBRATIONALLY EXCITED HYDROGEN
ON OXYGEN ATOMS

AND

EXCITATION OF HYDROGEN FLUORESCENCE
THROUGH NEAR-RESONANT ENERGY TRANSFER
FROM ARGON

BY

RICHARD N. DUBINSKY

A THESIS

Submitted to the Faculty of Graduate Studies
Through the Department of Chemistry in
Partial Fulfillment of the Requirements
For the Degree of Master of Science
At the University of Windsor

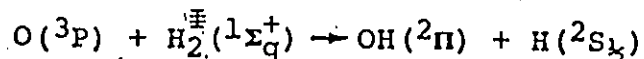
Windsor, Ontario
1976

© Richard N. Dubinsky 1976

In Memory of
John Palij (1898-1975)

ABSTRACT

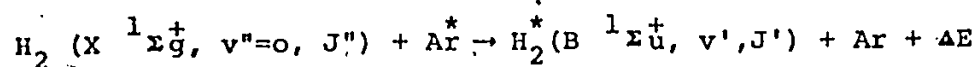
A preliminary study of the effect of vibrational energy on the rate of the reaction



was undertaken at 298°K in a pressure range of 114 to 322 Pa. Experiments were carried out using a discharge fast-flow system with a fixed observation port. Vibrationally excited hydrogen, H_2^\ddagger in an unspecified vibrational state was generated in a microwave discharge and reacted with O atoms formed by the $\text{N} + \text{NO} \rightarrow \text{N}_2 + \text{O}$ reaction under pseudo first-order conditions ($\text{O} \gg \text{H}_2^\ddagger$). Relative H atom concentrations were monitored using the atomic resonance fluorescence method at 121.5 nm. An approximate rate coefficient derived from the data can be expressed as $k^\ddagger \approx 8 \pm 5 \times 10^{10} \text{ cc mol}^{-1} \text{ s}^{-1}$. Calculation of a vibrational energy factor, α , leads to $\alpha \leq 0.50$ or no more than 50% of the vibrational energy of H_2 participates in overcoming the activation energy barrier.

Observations of the $v'=3, v''$ Lyman band progression from argon sensitized fluorescence of H_2 has been studied over a range of pressures. Quenching was observed at a partial pressure of hydrogen of about 50 Pa and a total pressure of 6×10^3 Pa, for transitions of

the type



where Ar^* is optically excited in the 3P_1 state and the H_2 molecules are initially thermally distributed over the J levels in the ground state. A simple mechanism is outlined which is consistent with the observations made in this investigation. There is also evidence that the energy transfer process produces hydrogen atoms with an efficiency of approximately 5% as important as production of H_2^* . More experimentation would be necessary in order to fully understand and substantiate the kinetics involved in this energy transfer process.

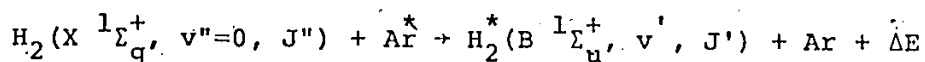
ABSTRACT

Etude préliminaire portant sur l'effet de l'énergie de vibration sur la vitesse de la réaction

$$\text{O}(^3\text{P}) + \text{H}_2(^1\Sigma_g^+) \rightarrow \text{OH}(^2\Pi) + \text{H}(^2\text{S}_{1/2})$$

a été entreprise à 298°K sous une pression échelonnée entre 114 et 322 Pa. Des expériences ont été exécutées en utilisant un système de décharge à flux rapide avec un point de observation fixe. De l'hydrogène d'excité par vibration, H_2 dans un état de vibration non spécifié était produite par une décharge de micro-ondes et réagissait avec des atomes d'O fixés par la réaction $\text{N} + \text{NO} \rightarrow \text{N}_2 + \text{O}$ sous des conditions de pseudo-premier ordre ($\text{O} > \text{H}_2$). Des concentrations relatives d'atomes H étaient contrôlées en utilisant la méthode la fluorescence de résonance atomique à 121.5 nm. Un coefficient approximatif de la vitesse dérivé des données peut être exprimé ainsi $k \approx 8 \pm 5 \times 10^{10} \text{ cc mol}^{-1} \text{ s}^{-1}$. Le calcul d'un facteur d'énergie de vibration, α , même à $\alpha \leq 0.50$ on a pas plus que 50% de l'énergie de vibration de H_2 qui participe à surmonter la barrière de l'énergie de l'activation.

L'argon sensibilise la fluorescence du spectre de bandes Lyman, $v' = 3$, $v'' \rightarrow H_2$. Cela a été étudié sur une étendue de mesures. L'amortissement était noté à une pression partielle de l'hydrogène d'à peu près 50 Pa et à une pression totale de 6×10^3 Pa, pour les transitions du genre



où l'Ar^{*} est excité optiquement dans l'état 3P_1 et les molécules d' H_2 sont d'abord distribuées thermiquement sur les niveaux J dans un état fondamental. Un mécanisme simple est présenté dans cette enquête. Il est compatible avec les observations faites ici. Il semblerait aussi évident que le processus de transfert d'énergie produit des atomes d'hydrogène avec une efficacité approximative de 5% aussi importante que la production de H_2^* . D'autres expériences seraient nécessaires pour comprendre à fond et pour justifier la cinétique de ce processus transfert d'énergie.

PREFACE

I would like to sincerely acknowledge the patience, support and expert guidance shown to me by my research adviser, Dr. Donald J. McKenney. His enthusiasm and positive attitude encouraged all aspects of this work.

Sincere gratitude is also extended to Dr. A. Van Wijngaarden for his help and guidance with the electronic and pumping systems, Dr. R. Rumfeldt and Dr. L. Hencher for helpful discussions and to Dr. M. Schlesinger for his advice on the rare gas continuum.

Special thanks must also be extended to Bob and Stella Pali, Barbara and Pat Whealan, Dr. Mike Quang Shen, James Miller, Frank Marentette, Tom Markham, Joanne Huneault and especially to Sonia Hyttenrauch and Cindy Pike for their friendship, support and elevating discussions.

The generous support of both the National Research Council of Canada and the University of Windsor, who provided financial aid during the period that this work was undertaken, is also gratefully acknowledged.

TABLE OF CONTENTS

	Page
ABSTRACT.....	ii
ACKNOWLEDGMENT.....	vi
LIST OF FIGURES.....	x
LIST OF TABLES.....	xii
GENERAL INTRODUCTION.....	xiii

Chapter

I	EXPERIMENTAL SECTION.....	1
	FLOW SYSTEM.....	1
	LAMPS AND DETECTING SYSTEM.....	5
	REAGENTS.....	7
	FLOW CALIBRATIONS.....	10

Chapter

II	PRELIMINARY STUDY OF H_2	16
	INTRODUCTION.....	16
	VIBRATIONALLY EXCITED HYDROGEN.....	18
	EXPERIMENTAL.....	19
	KINETIC ANALYSIS.....	21
	RESULTS AND DISCUSSION.....	22
	CONCLUSION.....	26

Chapter

III	NEAR RESONANT ENERGY TRANSFER FROM Ar TO H_2	29
	INTRODUCTION.....	29

	Page
EXPERIMENTAL.....	34
a) TECHNIQUES.....	34
b) PROCEDURE.....	35
c) SENSITIVITY.....	38
RESULTS.....	41
a) OVERALL OBSERVATIONS.....	41
b) INTERPRETATION OF RESULTS - LOW RESOLUTION STUDIES.....	47
c) KINETIC ANALYSIS:.....	47
(i) Low Pressure.....	49
(ii) High Pressure.....	51
d) PRODUCTION OF HYDROGEN ATOMS..	54
e) DETERMINATION OF [H]	55
f) HIGH RESOLUTION SPECTRA.....	59
CONCLUSIONS.....	68

Appendix

A	MICROWAVE-EXCITED ARGON EMISSION CONTINUUM...	73
	ARGON CONTINUUM LAMP.....	74
	ABSORPTION MEASUREMENTS.....	79

Appendix

B	DETECTING SYSTEM CALIBRATION.....	82
	MOLECULAR BRANCHING RATIO METHOD.....	84
	CALIBRATION OF DETECTION SYSTEM USED IN THIS WORK...	85

	Page
REFERENCES.....	92
VITA AUCTORIS.....	97

LIST OF FIGURES

Figure		Page
1(a)	Schematic Diagram of Pyrex Flow Tube.....	2
1(b)	Schematic top view of Fluorescence Observation Cell and Detection Section.....	3
1(c)	Schematic Diagram of Aluminum Fluorescence Cell, A.....	4
2	Schematic Diagram of Electronic Detecting.	7
3	Detection Efficiency of Channel Electron Multiplier.....	8
4	Calibration Graph for Hydrogen Flowmeter..	13
5	Decay Plot of Relative [H]	24
6	Relative Sensitivity of the Detecting System from 105 to 160 nm.....	40
7(a)	Transitions Between the Rotational - Vibrational Energy Levels for the (3,4) Band.....	42
7(b)	Pumping of the $v'=3, v''$ Level of the $B^1\Sigma_u^+$ State of H_2	42
8	Plots of Sensitized Fluorescence Intensity	43
9	Low Resolution Sensitized Resonance Fluorescence Spectrum of H_2	46
10	High Resolution Sensitized Resonance Fluorescence Scans.....	48
11	Plot of Resonant Fluorescence Intensity Relative to Atomic Hydrogen Fluorescence..	52
12	Calibration Curve Used in Determination of Absolute Concentration of Atomic Hydrogen.	58
13	Decay Plot of Lyman- α Fluorescence.....	62
14	Resonance Defects.....	63
15	Energy Defects.....	64

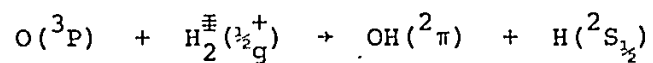
Figure		Page
16	Diagram of Microwave Discharge Lamp Used for Production of an Argon Continuum.....	75
17	Argon Continuum with Impurity Resonance Lines.....	78
18	Effect of Microwave Discharge at the Sidearm Containing Ba Getter on the Intensity Distribution of the Argon Continuum.....	80

LIST OF TABLES

Table	Page
1. Data Used for Determining Flow Rates for the hydrogen flowmeter.....	12
2. Summary of Kinetic Runs.....	23
3. Lowest Energy Levels of Argon Atom.....	30
4. Experimental Count Rates Observed for Bands.	45
5. Observed and Relative Intensities of Argon Sensitized Fluorescence of Hydrogen for $v' = 3, v'' = 4$ of Lyman Band Sensitized Fluorescence.....	60
6. Intensity Calibration of Relative Sensitivity of the Detecting Sysyem.....	90
7. Intensity Calibration of Relative Sensitivity of the Detecting System. (a) Normalized to $R(0)$. (b) P(2) branch of (3,4) transition.	91

GENERAL INTRODUCTION

This research was concerned with kinetic studies of the reaction



and also argon sensitized fluorescence of H_2 . Specific introductory comments relating to these studies are made in subsequent chapters but since most of the experimental details are common to both it seemed more convenient to begin with the experimental section which follows.

CHAPTER I
EXPERIMENTAL
FLOW SYSTEM

Energy transfer and kinetic experiments were carried out in a fast flow discharge apparatus. A movable injector assembly was used with a microwave discharge cavity for the generation of Hydrogen atoms H and/or vibrationally excited hydrogen H_2^{\ddagger} which can be measured at the base of the reaction column. Figures 1(a) and 1(b) are schematic diagrams showing the flow reactor and detection system.

$O(^3P)$ atoms were generated by the rapid reaction, $N + NO \rightarrow N_2 + O$, $k \approx 3 \times 10^{-11} \text{ cm}^3 \text{ molecule}^{-1} \text{ sec}^{-1}$ (1). H_2^{\ddagger} and N atoms were formed by passage through a 2.45 GHz microwave discharge (Microtron 200 or Raytheon) operated at 17-150W power output. A discharge bypass system, similar to that described by Clyne and Cruse (2) was used to obtain low concentrations of N.

NO was added at known flows through a jet approximately 10cm downstream of the N_2 discharge. The reactor flow tube was a 2.42 cm i.d. pyrex tube provided with a movable injector which was used for admitting the hydrogen at any position along the flow tube. The injector was fabricated from Vycor or Pyrex and its outer surface was treated with H_3PO_4 to inhibit O recombination and to act as a lubricant for the

FIG. 1. (a) Schematic diagram of the pyrex flow tube reactor. The sliding injector may be positioned at any point along the flow tube (2.42 cm i.d.); N_2 , flow of N atoms in N_2 carrier through D, discharge bypass; N_2 , Ar, main carrier gas flow; NOCl, NO, flow of titrants; P, connections to Silicon 704 oil manometer; L_1 , perpendicular resonance lamp; L_2 , Ar resonance lamp; H_2 , Hydrogen flow; T, tygon connector; D_1, D_2, D_3 , 2.45 GHz microwave discharges; A, aluminum block fluorescence cell (See Fig. 1. (c)); M, to monochromator and detecting electronics.

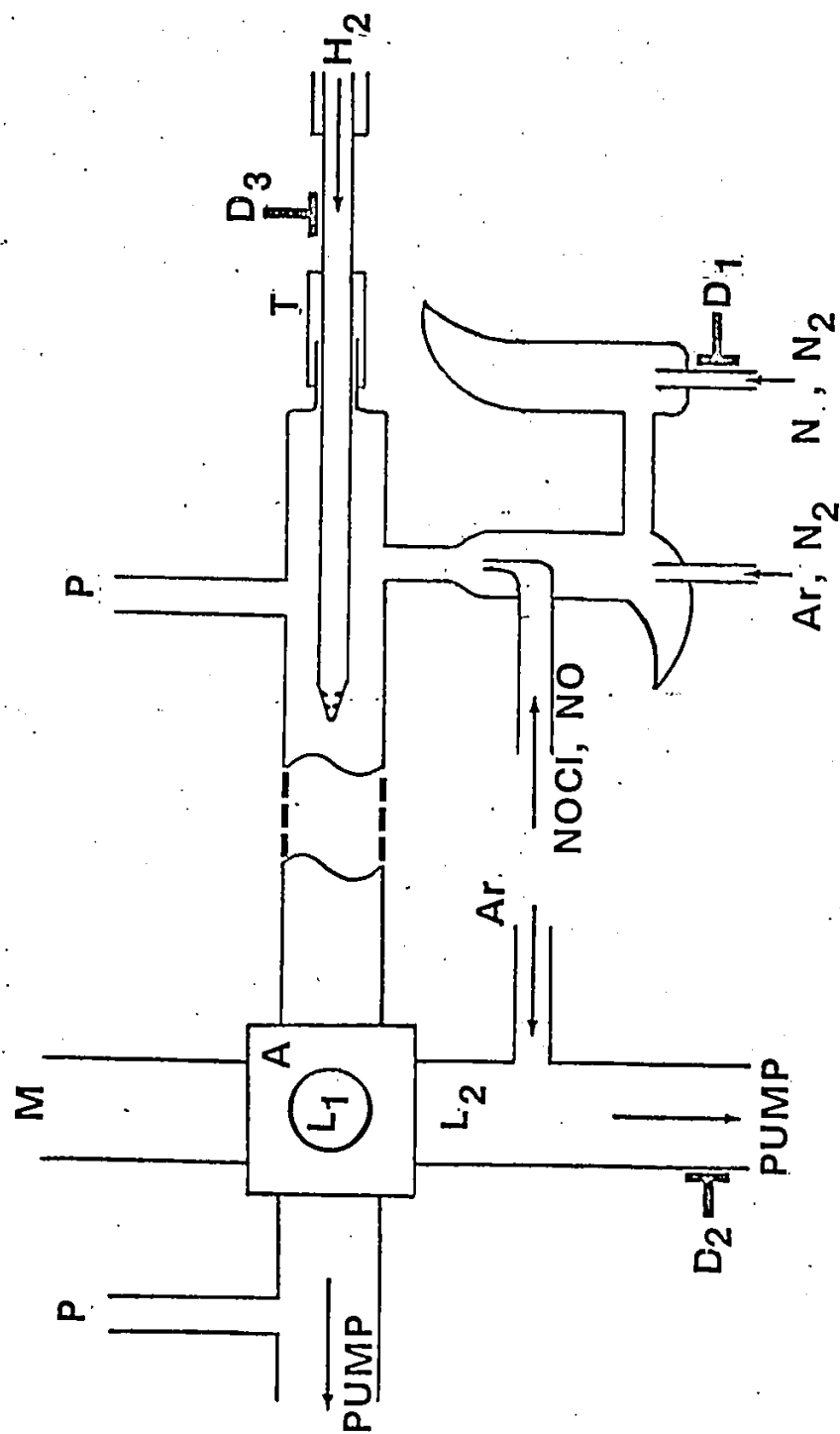


Fig. 1[a]

Schematic Diagram of Pyrex Flow Tube Reactor

FIG. 1. (b) Schematic top view of fluorescence observation cell and detecting system; L_1 and L_2 , resonance fluorescence lamps; M, monochromator; D, microwave discharge cavities; C_1, C_2 , Channel electron multiplier can be positioned at either one of two locations; I, Ion guage; O, Oxygen filter.

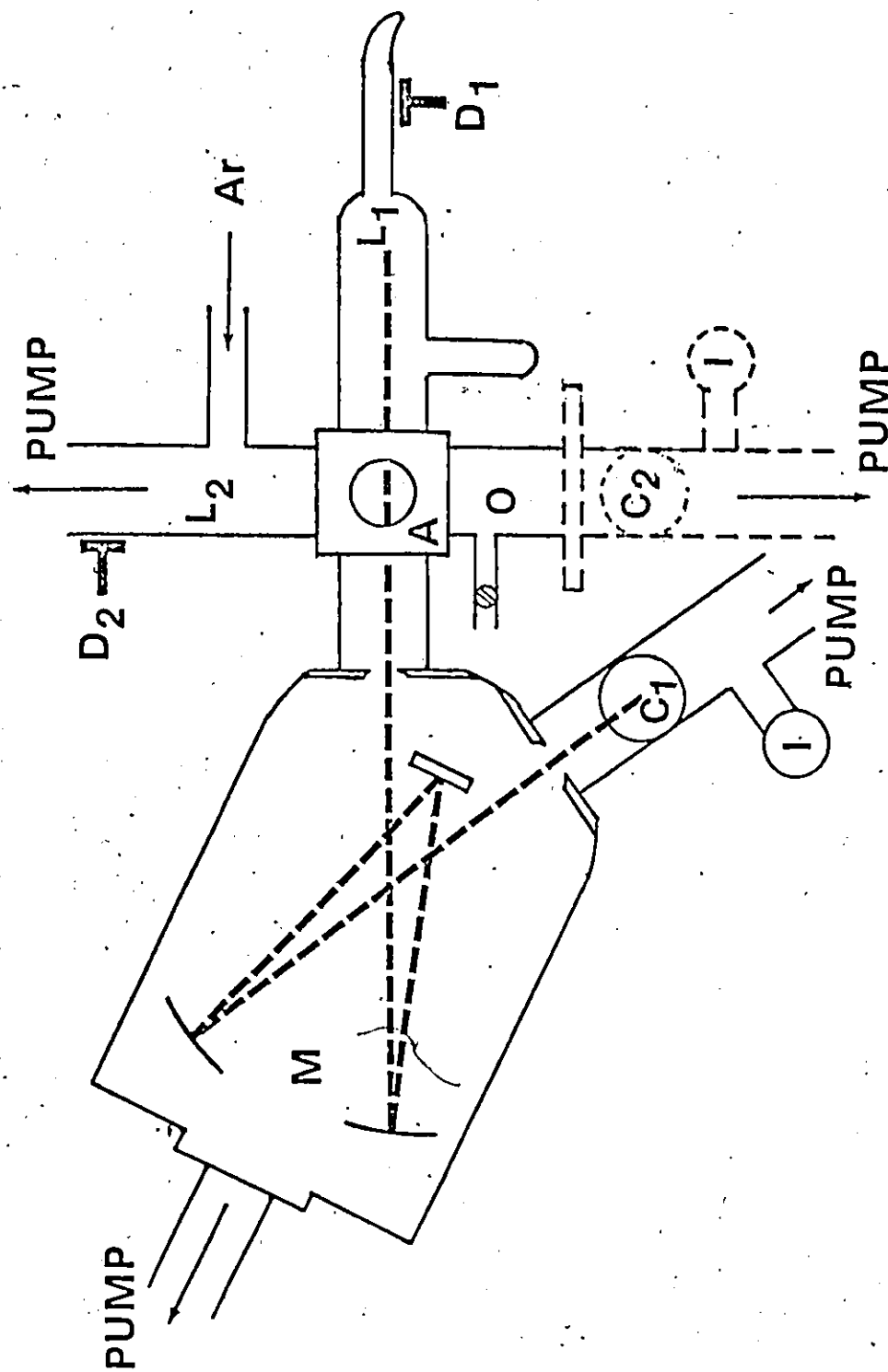


Fig. 1[b]

Schematic Top View of Fluorescence Observation Cell and Detection Section

FIG. 1. (c) Schematic diagram of aluminum fluorescence cell, A;
L₁, L₂, resonance lamps; M, monochromator;
C₂, Channel electron multiplier detector;
Flow, reactor column reagent fast flow system. LiF windows seal ends of L₁, L₂, C₂, M, to prevent interruption of flow. All ports are spaced 90° apart and support L₁, L₂, etc., with aluminum flanges fitted with Viton "O" rings. Dimensions of cell are 6.096 x 6.096 x 6.096 cm. along edges. The inner surfaces were all coated with Siliclad.

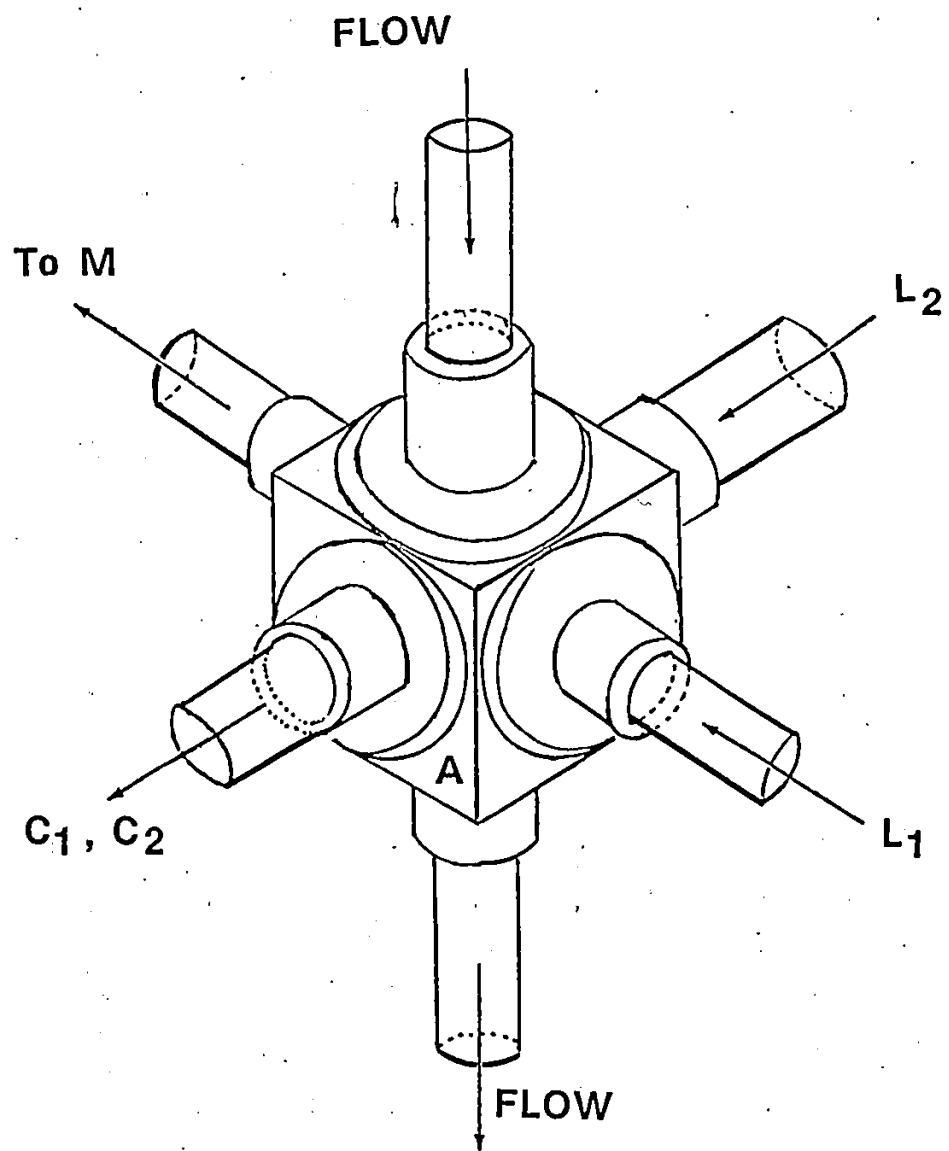


Fig. 1[c].

Schematic Diagram of Aluminum Fluorescence Cell, A.

tygon sleeve through which it passed. The interior of the injector remained untreated in most experiments in order to suppress formation of hydrogen atoms. The reactor column was internally coated in order to inhibit atom recombination.

The downstream end of the flow tube led through a large bore (2.0 cm) stopcock to a liquid nitrogen cooled high conductance trap followed by a Welch 500 l min⁻¹ (model 1397) rotary pump.

LAMPS AND DETECTING SYSTEM

The fluorescence cell was equipped with four polished LiF windows (Harshaw Manufacturing Co.). Severe transmission losses of the lithium fluoride window material occurred during experimentation that necessitated frequent changes of windows. The reason for this transmission loss has been attributed to LiF colour centres which is a critical problem when used near argon discharges. (see Fig.13 , page62).

Lamp L₂ was a low pressure Ar resonance lamp similar to that used by Bemand and Clyne (5), Lamp L₁ was a high pressure (27 kPa.) Ar continuum lamp similar to that described by Wilkinson and Byram, (4); a detailed treatment of the construction and application of this lamp appears in a later section under Appendix A. Cylinder argon, dried and purified by passage at low pressure through a liquid nitrogen-cooled trap packed

with molecular sieves (Davison 4 Å) and glass wool, flowed through lamp L₂ for excitation by means of a 2.45 GHz₂ discharge operated at ~17W. Total pressure in the lamp was maintained from 250 to 500 Pa for a typical flow rate of 1 μmol s⁻¹. The conditions used were chosen to maximize the signal to noise ratio.

The detecting system for sensitized and resonance fluorescence studies consisted of a McPherson monochromator (0.3m, model 218) with a 1200 line mm⁻¹ MgF₂ coated grating (blazed at 500 nm) joined to the flow reactor by a pyrex tube collimator which directs emitted radiation to the entrance slit. Detection was accomplished using a Bendix Channel Electron Multiplier (see Fig. 2) operated at 2800 V.d.c. (the power supply, Fluke, model 408B, specified line regulation of 0.001%) Signal pulses were amplified with a homemade preamplifier⁽ⁱ⁾ and an Ortec timing-filter amplifier (model 454). Counting rates were obtained after discrimination (Ortec integral discriminator, model 421); by either a rate-meter (Ortec model 441), chart recorder system or a digital counter (Ortec model 775), coupled to a variable timer (Ortec model 719). A complete schematic diagram of the electronic arrangement is given in Fig. 2. The detecting efficiency (6) of the Channel Electron Multi-

(i) Designed and constructed in the University of Windsor Physics Department electronic workshop.

FIG. 2. Schematic diagram of electronic detecting system.

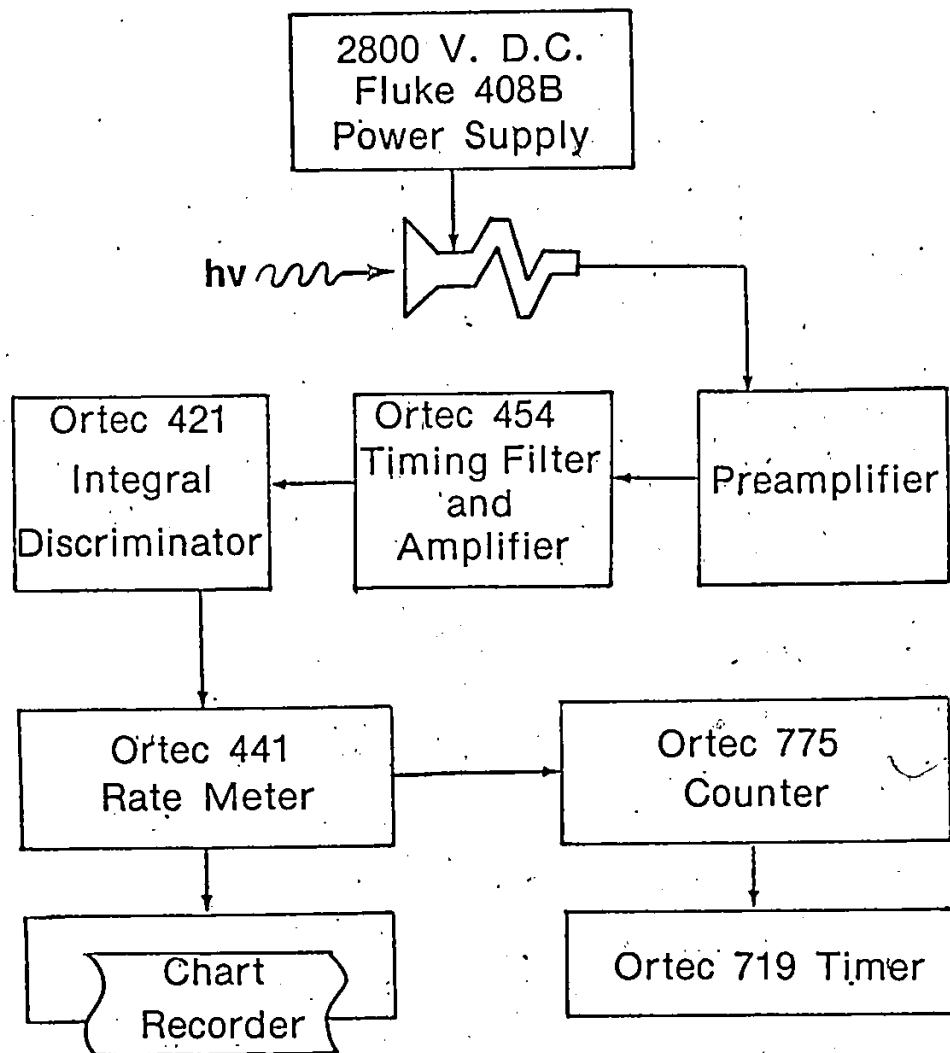


Fig. 2.

Schematic Diagram of Electronic Detecting System

FIG. 3. Detecting efficiency of Channel electron multiplier in ultraviolet region. (Ref. 6.)

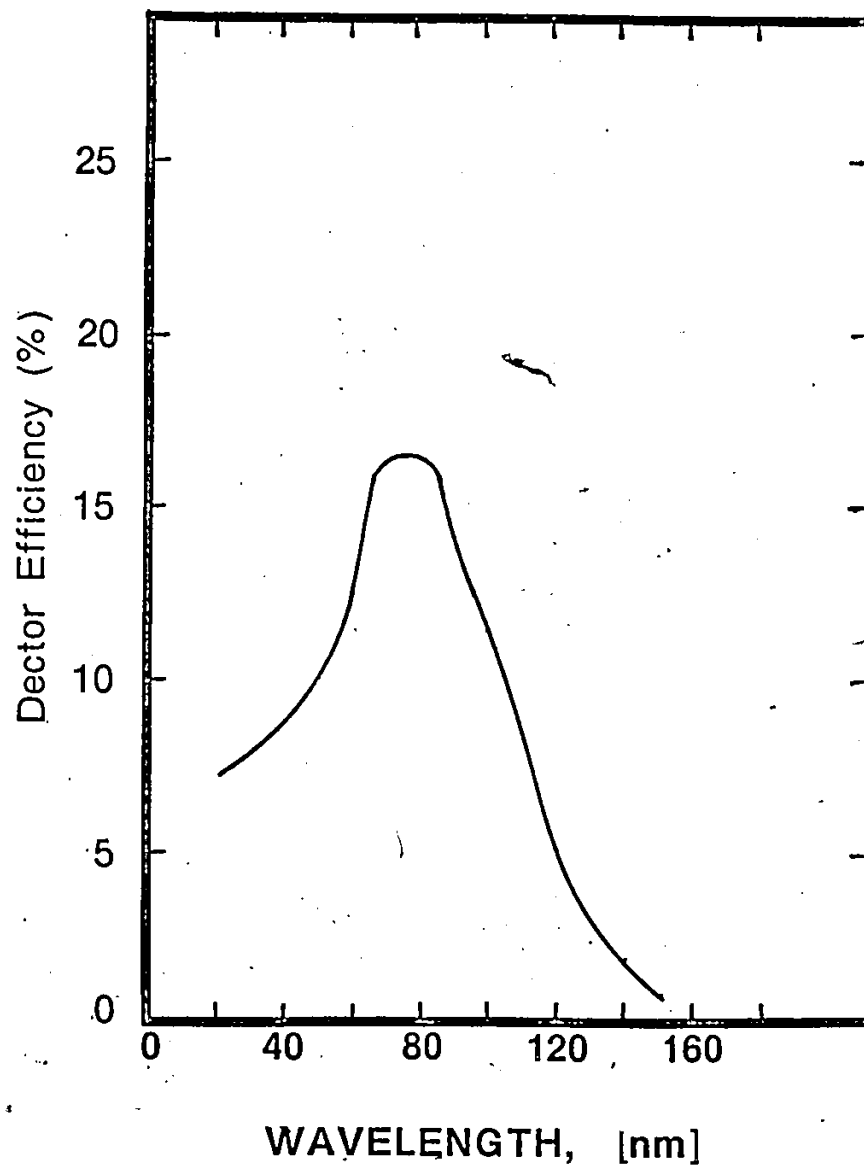


Fig. 3 .
Detection Efficiency of Channel Electron Multiplier

plier in the uv region is illustrated in Fig. 3. The detector was maintained at a pressure of approximately 7×10^{-5} Pa by a separate pumping system as shown in Fig. 1(b).

REAGENTS

Nitrogen (Liquid Carbonic) 99.996% stated purity was further purified by passage at 101.3 kPa pressure over copper (673°K), copper oxide powder (673°K), followed by a cold trap at 195°K. On the low pressure side of the flowmeter was another trap maintained at 77°K containing molecular sieves (Davison 4 Å) on glass wool. Tank argon (Liquid Carbonic) used for lamp L₂, was dried by passage at low pressures through a glass wool packed cold trap at 77°K. Ultra-pure Argon (Gas Dynamics) used for lamp, L₁, was similarly purified, then further purified with a Ba getter (Ventron Alpha) after lamp L₁ was sealed.

Ultra-pure hydrogen (Liquid Carbonic) was passed through a catalytic purifier (Deoxo-Englehard Mfg.) and a glass wool trap (77°K). Nitric Oxide and Nitrosyl chloride (Matheson) was distilled repeatedly under vacuum.

The base of the reaction column (fluorescence observation port) was taken as the approximate zero of the time scale (I_0) for the rate calculation, and the time, t , was given by the relation:

$$[1] \quad t = \frac{xAP}{RT \Sigma f}$$

where x is the length of the reaction column between the base of the column and the point of measurement. A is the crosssectional area of the flow tube ($A=4.63 \text{ cm}^2$), P is the total pressure, R is the ideal gas constant, T is the temperature in $^{\circ}\text{K}$ and Σf is the total flow of all gases.

FLOW CALIBRATIONS

All flows were measured using calibrated capillary flow meters. Calibration was carried out by monitoring the rate of pressure decrease ($\frac{dP}{dt}$) with time, inside a calibrated volume, V , concurrent with the effusion of the gas through the meter valve assembly (8). Flow rates were derived using the ideal gas equation,

$$[2] \quad \frac{dn}{dt} = \frac{dP}{dt} \cdot \frac{V}{RT}$$

where R is the ideal gas constant, and T is the temperature ($^{\circ}\text{K}$).

The calibration consisted of measuring the pressure decrease of gas from an isolated, precalibrated volume, V , as it flowed through the flow meter capillary-needle valve combination to the low pressure (pumped) side of the reactor. Pressure changes were arbitrarily chosen so that they were sufficiently small to insure a constant flow meter setting during a calibration run.

and large enough to facilitate accurate timing.

The flows were found to follow the Poiseuille relation for viscous flow:

$$[3] \quad \frac{dn}{dt} = \frac{\pi a^4}{8\eta l} \frac{(P_2^2 - P_1^2)}{RT}$$

in which dn/dt is the flow rate of a gas in moles s^{-1} , a is the radius of the flow tube, l is the tube length, η is the gas viscosity, R is the gas constant, T is the absolute temperature and P_2 and P_1 respectively are the high (backing) pressure, and low (reactor) pressure.

Equation [2] may be simplified (9) to:

$$[4] \quad \frac{dn}{dt} = K(2P - \Delta P) \Delta P$$

and plots of $\frac{dn}{dt}$ obtained from [2] are graphed according to equation [4]. A typical example using the hydrogen flowmeter will be given. Table 1 lists the results and Fig. 4 shows the calibration curve.

The calculations for the flowmeter capillaries were carried out by determining the pressure drop rate $\frac{dP}{dt}$ of a gas in the known volume, V , for a measured pressure difference ΔP through the flowmeter. The mass flow rate ($\frac{dn}{dt}$) was determined using equation [2] and [4].

Table 1. Data used for determining flow rates for the Hydrogen flowmeter. Values of dP/dt were obtained from the slope of a linear plot of pressure vs time graph carried out at various average pressures.

Notes from Table:

(a) Average pressure was determined by taking the arithmetic mean of the pressures used in a graph of P vs t for determination of the rate of pressure change dP/dt .

(b) $1 \text{ cm Hg} \equiv 1333.2 \text{ Pa}$

TABLE 1

Flow rate data

Average (a) Pressure (cm Hg) P_{avg}	Pressure drop in flowmeter (b) P (cm Hg)	$\frac{dp}{dt} \times 10^3$ (cm s ⁻¹)	$(2P - \Delta P) \Delta P$	$\frac{dn}{dt} \times 10^6$ mol s ⁻¹
46.17	0.19	21.06	17.53	15.76
54.25	0.28	38.88	30.30	29.08
49.60	0.13	17.34	12.88	12.96
45.30	0.43	45.70	38.77	34.18
57.65	0.07	11.28	8.07	8.44
52.52	0.35	46.20	36.64	34.54
43.85	0.56	58.82	48.80	44.00
45.90	0.28	31.54	25.63	23.59
40.32	1.08	104.69	85.92	78.31
38.75	0.90	87.50	68.94	65.45
38.95	0.74	70.30	57.10	52.58
36.15	0.44	41.02	31.62	30.68

FIG. 4. Calibration graph for Hydrogen flowmeter.

$$(1 \text{ cm Hg.})^2 = 1.778 \times 10^4 \text{ Pa}^2$$

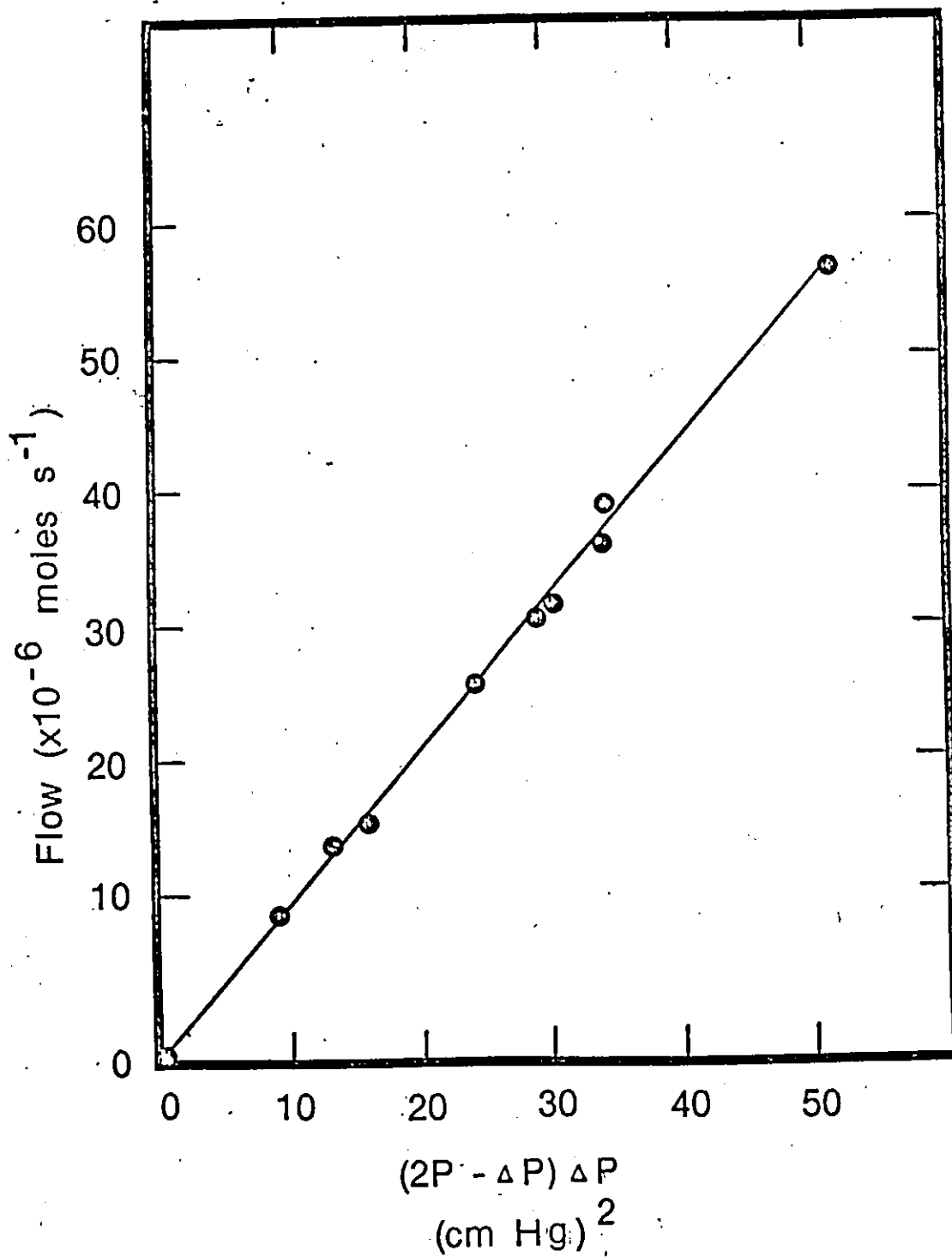


Fig. 4.
Calibration Graph for H₂ Flowmeter

$$V = 1409.8 \text{ cm}^3$$

$$R = 6.34 \times 10^3 \text{ (cm-ml)/(deg-mole)}$$

$$T = 297^\circ\text{K}$$

$$\frac{dn}{dt} = \frac{dP}{dt} (7.48 \times 10^{-4})$$

$$= K (2P - \Delta P) \Delta P$$

$$K = 0.917 \mu\text{mol s}^{-1} (\text{cm Hg})^{-1} \text{ for the hydrogen flowmeter.}$$

$\frac{dP}{dt}$ is taken as the slope from a linear graph of pressure vs. time for various average pressures. The average pressure P is used with the ΔP in the oil manometer in a plot with $(\frac{dn}{dt})$ or flow to obtain a linear plot, (see Fig. 4), from which flow may be read and used for subsequent calculations.

The partial pressure P_i of the reactants were calculated from the flow rates f_i by means of the expression:

$$[5] \quad P_i = \frac{f_i P}{\Sigma f}$$

The concentrations of the reactants were calculated from the partial pressures by utilizing the following relationship:

$$[6] \quad [i] = \frac{P_i}{RT}$$

The total pressure P , of the system was measured using a silicone oil manometer (1 cm oil = 10.40 Pa).

The concentration of NOCl and Ar were obtained by applying a gas velocity correction in lieu of recalibration since identical flowmeters were used and all other experimental conditions remained the same. The viscosity correction arose as a consequence of the assumption that all flows were viscous flows which obeyed the Poiseuille equation [3] .

It may be deduced from equation [3] that if two different gases pass through the same orifice under identical experimental conditions, the ratio of their flow rates will be inversely proportional to the ratio of their viscosities. Viscosity data was taken from the CRC Handbook (7) .

CHAPTER II

INTRODUCTION

Rate accelerations for chemical reactions have been observed for the case where one of the collision partners is vibrationally excited (10), (11), (12), (13). Birely and Lyman (14) reviewed all the vibrationally enhanced reaction results obtained in hopes of showing a correlation between the magnitude of the vibrational enhancement of rate processes and identifiable physical variables. They concluded that there was insufficient experimental data to adequately test the theoretical treatments (15), (16), (17).

Theoretical treatments based on the concept of microscopic reversibility (15), (16), (17) require more data than is presently available (14) and there is no obvious way in which to formulate the vibrational acceleration of rate processes in terms of easily measured microscopic or macroscopic variables. It was proposed (14), however that excess reactant vibrational energy E_v , can be used to overcome the Arrhenius activation energy E_a . In this case, the rate constant, k^\ddagger for reaction of vibrationally excited reactants is increased by a factor of $\exp \left(\frac{E_v}{RT} \right)$ above that for reactants in their ground state. The efficiency in using internal energy to overcome the Arrhenius activation energy, E_a is measured by the parameter α and is defined by:

$$[7] \quad E_a^\ddagger = E_a - \alpha E_v$$

Assuming that A^\ddagger , the Arrhenius pre-exponential factor remains unaffected by the degree of excitation of the internal reactants; it is possible to calculate α from the ratio $(\frac{k^\ddagger}{k})$ as:

$$[8] \quad \alpha = \frac{RT}{E_v} \ln\left(\frac{k^\ddagger}{k}\right)$$

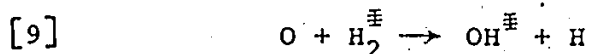
The Arrhenius factor is assumed to be unaffected primarily due to the lack of data on the bulk temperature dependence of k^\ddagger . It is also emphasized that the conversion efficiency parameter, α is an empirical quantity used only as an indication of the vibrational acceleration of rate processes. Reactions of vibrationally excited H_2 , HCl , OH and O_3 exhibit rate acceleration attributable to vibrational energies (10)-(14) with $\alpha \leq 0.6$ in all cases.

There has been no obvious correlation of α to the energetics of vibrationally enhanced systems that have been studied. It has been indicated (18) that the reagent vibrational energy is generally more effective than translation in promoting endothermic reactions whereas the contrary is indicated for the exothermic system. For all the exothermic systems recently studied, $\alpha < 1$, however there is no strong relationship between α and ΔH . There is some indication for reactions of HCl^\ddagger that α increases with increasing mass of

the atomic reagent.

VIBRATIONALLY EXCITED HYDROGEN

Reactions involving vibrationally excited hydrogen H_2^{\ddagger} , are of interest for both theoretical and practical reasons. In particular, the reaction of vibrationally excited hydrogen H_2^{\ddagger} , with ground state atomic oxygen (3P) is important to our atmosphere as well as in outer space. Recent measurements related to missile exhausts indicate significant IR radiation from vibrationally excited hydroxyl radicals (OH^{\ddagger}) created by a non-carbon burning fuel (19). This excitation has been attributed to the reaction:

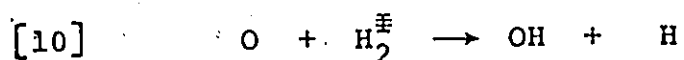


It has also been suggested that vibrationally excited H_2^{\ddagger} plays an important role in upper atmosphere photochemistry (20). If a significant level of H_2^{\ddagger} is present above 50 km, calculations show the buildup of H_2 appreciably reduced and a large increase in H_2O near the mesopause.

The energy difference between the zeroth and first vibrational levels of H_2^{\ddagger} is very large (ie 49.8 kJ mol^{-1}). If all of the vibrational energy were used in overcoming the 36.0 kJ mol^{-1} measured activation energy (21) for the reaction between molecular hydrogen and atomic oxygen,

$$O + H_2 \rightarrow OH + H$$

then the reaction should be very fast and a flowing stream of oxygen atoms would be rapidly depleted by the addition of vibrationally excited hydrogen, H_2^{\ddagger} . (By H_2^{\ddagger} we mean $X \sum_g^+ H_2$ in an unspecified vibrationally excited state).



A fast flow discharge system utilizing a resonance fluorescence detecting technique for monitoring H production and O depletion was used to study the influence of vibrational excitation of H_2^{\ddagger} on the rate of reaction [10] at 298°K.

EXPERIMENTAL

A detailed discussion and thorough description of the experimental apparatus used in these experiments was given in the preceeding chapter. This section only briefly describes the techniques in studying this reaction.

A great deal of effort was made in an attempt to directly observe and monitor vibrationally excited H_2^{\ddagger} ($v=1$) by absorption. For this purpose an Argon continuum lamp was constructed (see Appendix A) to serve as a radiation source. H_2^{\ddagger} ($v=1$) absorbs from 112.0 to 117.4 nm (22). Fig.17 shows the spectrum of the Argon continuum observed. It is apparent that the transmission below 115.0 nm was insufficient to

successfully observe H_2^{\pm} ($v=1$) absorption. (i) Nevertheless, some preliminary runs were carried out as follows.

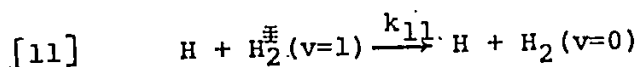
Initially the reaction [10] was studied by discharging gaseous molecular Hydrogen (Liquid Carbonic Ltd.) in an injector assembly (see Fig. 1(a)), and reacting the products with $O(^3P)$ created by the chemiluminescent reaction $N^* + NO \rightarrow N_2 + O$ while monitoring the production and decay of relative H by either of the two following techniques; (i) resonance fluorescence observed through an oxygen filter and (ii) by monochromatization of the resonant fluorescence at $\lambda = 121.6$ nm.

Signals were generally found to be erratic and quite often only slightly above noise levels and critically depended on column coatings used to inhibit recombination of the H atoms produced.

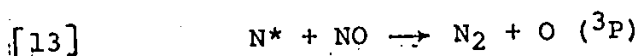
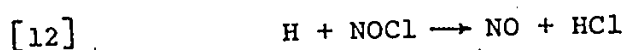
Photon counts utilizing the Ortec Model 775 counter were usually taken for durations of 60 seconds for each measurement during a run. A run comprised about 50 measurements. Reaction times ranged from about 3 to 14 milliseconds and the data collected over this range consisted of graphs that showed a general increase in intensity towards longer reaction times as expected.

(i) The monochromator has now been returned to the factory for refurbishing, cleaning and recoating the optics.

R. F. Heidner III (22) observed that kinetic experiments on the deactivation of H_2^{\ddagger} ($v=1$) strongly favours the gas phase process over a wall deactivation process. A rate constant, $k_{11} = 1.8 \pm 0.9 \times 10^8 l \text{ mol}^{-1} \text{ s}^{-1}$ was obtained for the following process:



In order to minimize this effect, a reaction with NOCl was carried out to eliminate H and provide a means of obtaining O by reaction of $N^* + NO$.



Unfortunately the concentration of O obtained by this method was too low to observe visually (air afterglow) and no pronounced reaction with H_2^{\ddagger} was observed in fluorescence measurement of either H or O.

KINETIC ANALYSIS

Preliminary values of k^{\ddagger} were derived from the following equation based on reaction [10],

$$[14] \quad \frac{-d[H_2^{\ddagger}]}{dt} = \frac{d[H]}{dt} = k_{10}^{\ddagger}[O][H_2^{\ddagger}]$$

Pseudo first-order conditions were assumed with $[O] > [H_2^{\ddagger}]$. It is emphasized however that without a valid measure of H_2^{\ddagger} such an assumption is not wholly justified. However, in other studies (22) $[H_2^{\ddagger}]_0$ had been estimated as approximately equal to $[H]_0$. In

this work $[H] < [O]$ and from [14] .

$$[15] \quad \frac{d(\ln [H_2^{\ddagger}]_0 / [H_2^{\ddagger}])}{dt} = k_{10}^{\ddagger} [O]$$

and since $[H]$ produced = $[H_2^{\ddagger}]$ removed

$$[16] \quad \frac{d(\ln [H] / [H]_0)}{dt} = k_{10}^{\ddagger} [O]$$

The ratio $[H] / [H]_0$ is given by the measured ratio of L- α fluorescence intensities I / I_0 in the absence of (I_0) and presence of H_2^{\ddagger} (I).

RESULTS AND DISCUSSION

The results of all the runs are listed in Table 2 and typical H atom fluorescence decay plots are shown in Fig. 5. From this data a very preliminary estimate of k_{10}^{\ddagger} was derived ($k_{10}^{\ddagger} \approx 8 \pm 5 \times 10^{10} \text{ cc mol}^{-1} \text{ s}^{-1}$).

The extremely poor precision in these data is probably due to loss of H, and H_2^{\ddagger} deactivation on the walls of the flow reactor. In addition if $[H_2^{\ddagger}] \approx [O]$ a second-order kinetic analysis would be appropriate.

Clearly before a reliable value could be obtained, $[H_2^{\ddagger}]$ must be measured. Nevertheless it is interesting to compare the value obtained here with the only published (11) estimate. ($k_{10}^{\ddagger} \leq 6 \times 10^{10} \text{ cm}^3 \text{ mol}^{-1} \text{ s}^{-1}$). Birely et al (11) used vacuum ultraviolet fluorescence for monitoring the concentrations of major species. No H atoms were detected in the resonance fluorescence cell when O

Table 2. Summary of kinetic runs.
(Preliminary Results)

TABLE 2

Summary

Total pressure Pascals (Pa) ($\times 10^1$)	$[H_2]_0$ mol cc ⁻¹	$[O]_0$ mol cc ⁻¹	$\frac{d \ln([H]/[H]_0)}{dt}$ s ⁻¹	k^{\ddagger} Rate constant cc mol ⁻¹ s ⁻¹
15.1	1.13×10^{-8}	3.80×10^{-11}	14.71	3.87×10^{11}
15.1	1.13×10^{-8}	3.80×10^{-11}	12.44	3.27×10^{11}
15.1	1.03×10^{-8}	1.59×10^{-10}	21.16	1.33×10^{11}
18.7	1.06×10^{-8}	1.57×10^{-10}	12.54	7.99×10^{10}
25.0	1.33×10^{-8}	2.48×10^{-10}	8.11	3.27×10^{10}
32.2	1.57×10^{-8}	3.44×10^{-10}	4.62	1.34×10^{10}
18.7	9.31×10^{-9}	1.15×10^{-10}	12.90	1.12×10^{11}
14.6	6.68×10^{-9}	1.27×10^{-10}	9.26	7.29×10^{10}
18.7	1.17×10^{-8}	9.64×10^{-11}	6.33	6.56×10^{10}
15.6	1.26×10^{-8}	3.01×10^{-10}	2.19	7.28×10^9
11.4	2.91×10^{-9}	6.73×10^{-11}	3.22	4.79×10^{10}
14.6	2.34×10^{-9}	4.57×10^{-11}	0.48	1.04×10^{10}
14.6	2.33×10^{-9}	1.75×10^{-10}	1.67	9.54×10^9
13.5	3.92×10^{-9}	3.42×10^{-10}	3.18	9.29×10^9
13.5	3.91×10^{-9}	4.27×10^{-10}	3.46	8.11×10^9
13.5	6.00×10^{-9}	2.95×10^{-10}	1.50	5.07×10^9
				$k_{avg}^{\ddagger} = 8(+5) \times 10^{10}$

FIG. 5. Decay plot of relative H .
 $P_{\text{tot}} = 32.2 \text{ Pa}$; $[H_2]_0 = 1.57 \times 10^{-8} \text{ mol cc}^{-1}$;
 $[O]_0 = 3.44 \times 10^{-10} \text{ mol cc}^{-1}$;
Slope = 4.62 s^{-1} ; $T = 298^\circ \text{K}$.

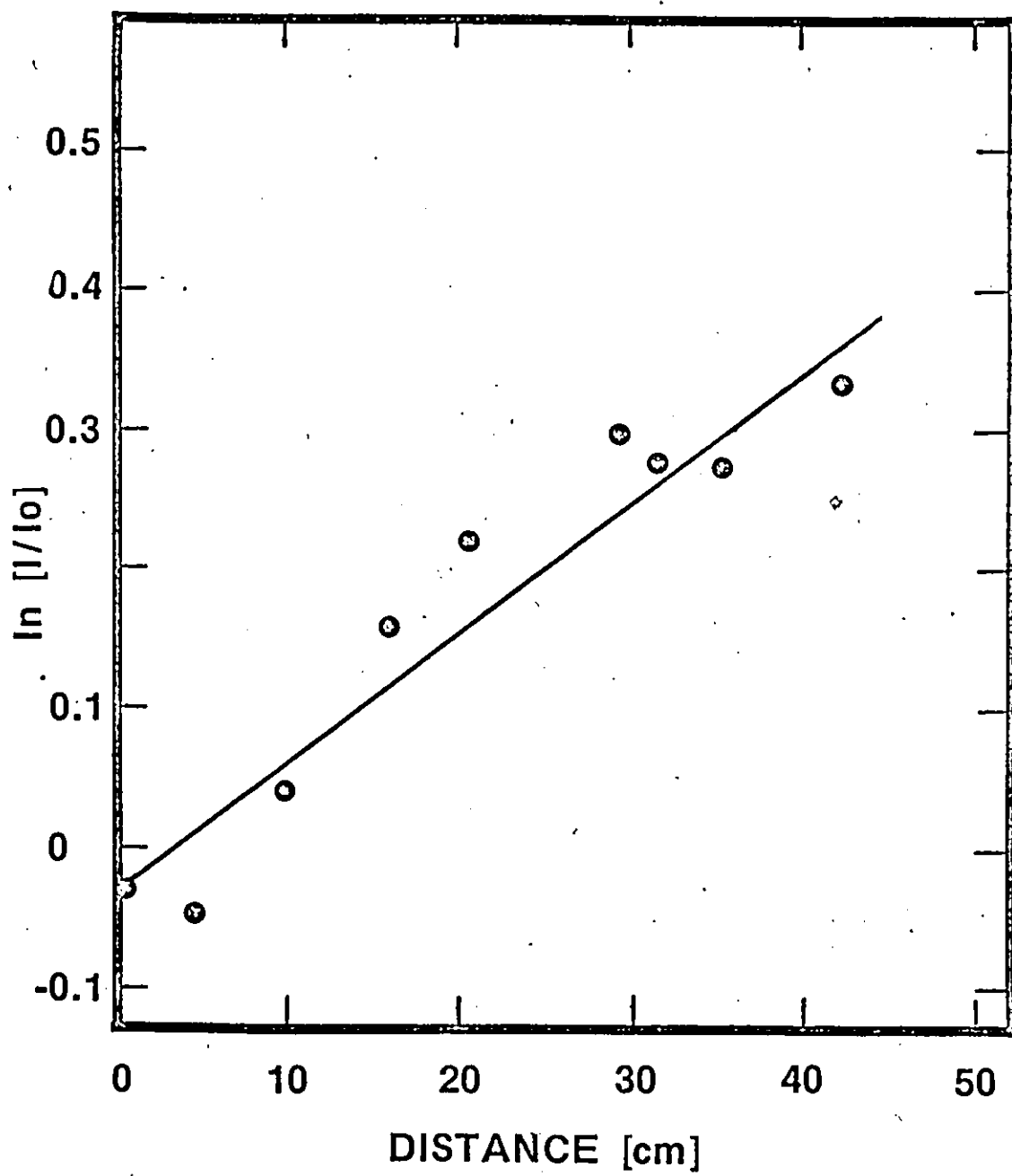


Fig. 5.
Decay Plot of Relative (H)

atoms were mixed with H_2^{\ddagger} . Also, addition of H_2^{\ddagger} led to no detectable change in the fluorescence by O. Furthermore, addition of O had no detectable effect on the concentration of H_2^{\ddagger} . The explanation for this behaviour was attributed to a lack of sensitivity in the detection system since the smallest increment in the H atom density that was detectable was $10^{-11} \text{ mol cm}^{-3}$. Saturation of O atom resonance absorption occurred for $[O] = 1.6 \times 10^{-10} \text{ mol cm}^{-3}$, similarly for $[H_2^{\ddagger}]$, hence only an approximate value on k_{10}^{\ddagger} could be established.

From the observed results, it is clear that the total measured activation energy cannot be overcome by the vibrational energy of $H_2^{\ddagger}(v=1)$. By assuming that the Arrhenius pre-exponential factor is identical for the reaction of both ground state and excited H_2^{\ddagger} , we can roughly estimate the fraction α of the H_2^{\ddagger} vibrational energy, E_v , used in overcoming the activation energy E_a . Using the previously determined value of k (21), (Resonance fluorescence) for the reaction between ground state hydrogen and oxygen ($k = 2.33 \times 10^6 \text{ cc mol}^{-1} \text{ s}^{-1}$) at $T = 298^\circ\text{K}$ we can write the relationship between the reaction with excited and ground state Hydrogen as:

$$[17] \quad \frac{k_{10}^{\ddagger}}{k} = \frac{8 \times 10^{10}}{2.33 \times 10^6} = \exp(\alpha E_v / RT)$$

from which, $\alpha \leq 0.5$

Hence no more than $\approx 50\%$ of the vibrational energy of H_2^{\ddagger} is used in overcoming the activation energy. This

is in agreement with the work of Birely et al. (11), who calculated $\alpha = 0.53^{(i)}$. This is also in agreement with other recent studies (14) for which α is generally less than 0.6.

CONCLUSION

These preliminary experiments concerned with H_2^{\pm} allow much room for improvement. Monitoring $[H_2^{\pm}]$ is necessary to fully establish the extent of reaction of this species with oxygen atoms.

Since resonance fluorescence has been shown to be applicable for concentrations as low as 5×10^{-15} mol/cc (23), (24) it would seem that this technique would offer a very sensitive means of determination of H_2^{\pm} under the proper conditions. The existence of vibrationally excited ground state hydrogen in the $v''=1$ or $v''=2$ levels would be manifested as sensitized near resonant fluorescent emission if an argon lamp is used for excitation. The R(1) line at 106.7 nm of the $v'=10, v''=2$ band of the $(B^1\Sigma_u^+ \rightarrow X^1\Sigma_g^+)$ transition is nearly identical to the Argon resonance line at 106.7 nm which is strongly excited in an Argon resonance lamp (27). This progression can be observed as sensitized fluorescence radiation and is nearly identical to the process used by Wood in his experiments with Na_2 (25).

(i) α was incorrectly reported as 0.3 in ref (11) and (14), personal communication.

Resonance excitation is demonstrated as the process causing this enhancement observed in the following part of this thesis. Since the resonance defect of the B_{10}^2 level is very small, ($\Delta v=0.7$, see in Ar section, p.63) a strong excitation of this level in collision with excited Ar in the 3P_1 state with H_2^{\ddagger} in the x_2^1 level would produce this characteristic enhanced progression $v''(v'=10)$ from 98.2 nm to 150.0 nm as observed in discharges by Takezawa et al (28), Beutler (29), (30) and Herzberg et al (26).

Takezawa et al (28) proved the existence of $v=2$ of the ground state for vibrationally active H_2^{\ddagger} by observing the absorption spectrum of H_2^{\ddagger} which was discharged downstream in a flow system. This was not able to be observed in this experiment due to the insensitivity of the optics and the large concentrations of H_2^{\ddagger} required (see Appendix A). Sensitized resonance fluorescence originating from the vibrationally excited ground state hydrogen $v=1$ (x_1^3, x_1^2) exemplifies itself as emission from the C state ($v'=0, v''$) of H_2 (excited by the 1P_1 state of Ar) which emit from 101.0 - 119.2 nm. The energy defects in this case (28) are very similar to those for the Lyman bands $v''(v'=3)$ however, the emission is in a less sensitive range than can be observed in our detecting system. In order to observe vibrationally excited hydrogen, a long absorption cell would be required and high sensitivity in the region from 105.0 - 110.0 nm for $v=1$, well resolved emission, and a low

pressure-powerful lamp discharge. Sensitized fluorescence would serve as a more desirable technique, however a more sensitive detection apparatus would be required in the far uv.

The importance of the effects of vibrational excitation on reaction rates cannot be underestimated. If H_2^{Ξ} constitutes a major product from H_2 discharges, then this will have to be taken into consideration for all previous and future studies carried out utilizing this technique. The elucidation of the behaviour of excited species will also have the effect in determining the importance of these reagents in our atmosphere.

CHAPTER III

INTRODUCTION

Absorption of energy by collisions of excited particles with a neutral atomic or molecular gas can lead to energy transfer phenomena producing excited states and ionic species, (31).

The interaction of radiation with a system which absorbs energy leads to a new chemical and thermodynamic equilibrium by a number of intricate processes. Precise information concerning the dissipation of energy in various gases is needed because of its direct application to important excitation mechanisms of gas laser systems (32) and radiation chemistry as well as contributing to knowledge concerning atmospheric processes of our own and other planets.

Increasing interest has recently been given to electronic energy transfer reactions (33) - (39). A number of studies carried out in recent years have been concerned with analysis of the product channels between metastable argon atoms and a variety of small molecules. Particular interest has been paid to analysis of electronically excited product states (33), (40).

The use of noble gases in energy transfer research is fundamentally important. A number of important pathways are available for energy distribution; among these is the transport of resonant or near resonance radiation.

The number of possible energy pathways is more limited for the inert gases than for molecular species and their inert chemical properties makes gases such as argon an excellent species with which to study energy transfer reactions. A study by Thonnard and Hurst (41) contributed much to the awareness that both metastable states and resonance states are very important in the energy pathways for noble gases.

Many resonance radiation studies (41), (42), (33) utilize the first excited electronic configuration of Argon ($3p^5 4s^1$) (35) which gives four increasingly energetic states, $^3P_{2,1,0}$ and 1P_1 . Transitions of the resonance states, 3P_1 and 1P_1 to the ground state are allowed for electric dipole radiation and follow the selection rules $\Delta J = 0, \pm 1; J = 0 \nrightarrow 0$. The spectroscopic notation and energy levels (35) are shown in Table 3.

TABLE 3

Lowest energy levels of Argon atom (a)

SPECTROSCOPIC NOTATION		nm	kJ mol^{-1}
R-S	Moore		
1P_1	$1s_2$	104.8	
3P_0	$1s_3$	105.8	1130.9
3P_1	$1s_4$	106.7	
3P_2	$1s_5$	107.4	1114.2

(a) Reference 35.

Introduction of a foreign molecule or atom perturbs the complicated relaxation of the excited system by introducing new pathways depending on the nature of the added gas. Precise calculations on the hydrogen molecules (43), (44) have inspired reinvestigations of the Lyman bands for H_2 and its isotopic species. Much improved resolution and wavelength accuracy has been achieved (45) since the pioneering experiments of Theodore Lyman (46).

Early studies by Lyman (46) and others (47), (48) demonstrated that the normally complex emission spectrum of H_2 in the vacuum-ultraviolet region is considerably simplified upon the addition of an excess of Ar. Lyman (46) observed that the single progression ($v'=3, v''$) of the $B \ ^1\Sigma_u^+ \rightarrow X \ ^1\Sigma_g^+$ band system of H_2 was very much enhanced whereas other bands were very much weakened in the presence of Ar in a discharge.

Other investigators found similar results but with some differences also noted. Beutler (29) found an additional progression of the Lyman bands i.e. ($v'=10, v''$) in a similar system with HD, however for this second transition, the individual bands only originated from the $J=2$ rotational level of the upper state (i.e. only the R(1) and P(3) branches were seen).

K. Mie (49) observed similar phenomena to the Beutler progression; the $v'=3, v''$ progression was observed but contrary to the Lyman observation on H_2 , the

individual bands contained transitions emanating from both $J=1$ and $J=2$ levels of the upper states, i.e. the $R(0)$, $R(1)$, $P(2)$ and $P(3)$, with the $R(0)$ unresolved from the $R(1)$ line. The ($v'=0$, v'') progression of the Werner bands, $C^1\Pi_u \rightarrow X^1\Sigma_g^+$ for HD was likewise enhanced (49).

Witmer (47) observed that for a very low partial pressure of H_2 in Ar, this progression ($B^1\Sigma_u^+ \rightarrow X^1\Sigma_g^+$) appears with almost no association of extra bands. Dieke and Hopfield (48) suggested that the enhancement may be due to collisions of the second kind (i.e. excited atoms collide with slow electrons and produce unexcited atoms and fast electrons (50) with metastable argon atoms but they did not specify the two metastable states in their work. Beutler (30) also studied this progression but was not able to resolve the problem (28).

The theoretical explanation first developed by Kallmann and London (51), is more generally explained by N. F. Mott and H.S.W. Massey (52) as the theory of resonance excitation. Essentially the $v'=3$ level of the B state of hydrogen is selectively excited by collision of argon (106.6 nm) with ground state H_2 .

From Kallmann and London's theory (28), (51) the upper level of the enhanced bands, $v'=3$ of $B^1\Sigma_u^+$, should be selectively excited by collisions of Ar atoms in the 3P_1 state and not in the metastable state as suggested by Dieke and Hopfield (48). The efficiency of this excitation should follow optical selection rules

and be proportional to the resonance defects (28).

This is in agreement with S. Takezawa et al. (28) who confirmed the K-L theory in their observations.

Considerable interest has centered on the selective enhancement of the H_2 spectrum in the vacuum ultraviolet region when excited with an Ar resonance lamp in an atmosphere of argon. Excitation of the hydrogen molecules into specific vibrational and rotational levels of the B $^1\Sigma_u^+$ electronic state is explained by the absorption of the 104.8 and 106.6 nm argon resonance lines (40) and by near-resonant electronic energy transfer from excited argon to hydrogen (33). All the early experiments of selective enhancement were carried out with both H_2 and Ar present in the exciting lamp (46), (28), (27). Only recently has the H_2 source been separate from the lamp (33), (40).

Fink et al. (33), (40) used two different experimental arrangements in which hydrogen was excited in a fluorescence cell outside of the discharge zone. This allowed them to use a single emission line of the lamp for excitation and to measure the unresolved molecular fluorescence intensity or to observe the resolved fluorescence radiation spectroscopically.

This work was carried out for confirmation of Fink et al.'s observations and to investigate the possible dissociation of H_2 into hydrogen atoms as an effective collision channel which may compete with energy transfer.

EXPERIMENTAL

a) TECHNIQUES

Techniques utilizing resonance fluorescence have been explored for a number of years and have become established (50), (52), (53) in energy transfer experiments.

Hydrogen is a simple system where the interaction of only two electrons must be considered. The hydrogen molecule is particularly favourable because of its widely spaced energy levels. The resonance-fluorescence method of studying energy transfer between Ar and H₂ has been employed in this study. Collisions between optically excited argon atoms and hydrogen molecules produce excitation of the nearly resonant electronic-vibration-rotation state ($B^1\Sigma_u^+$, $v'=3$, $J'=0 \rightarrow 4$) of H₂ for relatively high total pressures (up to 20kPa). At these pressures, spontaneous emission, in the vacuum ultra-violet region, return the molecules to the ground electronic state ($X^1\Sigma_g^+$) from the excited level. The experimental procedure administers a mixture of hydrogen and argon which is excited by an argon resonance lamp.

Hydrogen radiates with a lifetime of approximately 8×10^{-10} seconds (54). The rate constant for collisional processes can be established by measuring the observed fluorescence spectra over a wide range of pressures and using the known radiative transition rates (55) to establish the time scale for excitation of the hydrogen into (i) rotational (ii) vibrational, and (iii) electro-

nic states.

b) PROCEDURE

The detection system; fluorescence cell, lamp, monochromator, Channel Electron Multiplier, electronics, and recorder are described in Chapter I. Typical pressures in the resonance fluorescence lamp that were required in order to produce the H_2^* B state, was approximately 0.4 kPa. This is much higher than that used by Fink et al. (33) who used 6×10^{-4} kPa, however at lower pressures than ≈ 0.1 kPa, no signal could be observed in our apparatus and the optimum pressure for Lyman band fluorescence was experimentally determined to be in the vicinity of 0.2 - 0.5 kPa Ar pressure in the lamp. This was determined by setting the wavelength of the monochromator to a peak corresponding to a transition of the Lyman band in the fourth order (usually the R(0) branch of the (3,4) transition at 126.9 nm) with an Ar/ H_2 mixture either flowing or under static conditions. The Ar flow through the lamp was then adjusted to a point where this signal reached a maximum. This procedure was carried out before each run.

Scans were then taken in the fourth order over the wavelength range 100.0 nm to 165.0 nm at scan rates of 0.1 to 2.0 nm min⁻¹. The optimum scan rate for maximum resolution was found to be 1.0 nm min⁻¹.

Alternatively, once the exact wavelengths of the

Lyman bands were determined, the wavelength of the monochromator was set at the corresponding peak and count rates using the Ortec discriminator and counter were undertaken for periods of 1 min. In this method, the intensity of Lyman - α emission in the fourth order (121.5) was monitored for 1 minute after each measurement of a Lyman-band peak. Count rates were normally taken until two successive count rates agreed within statistical deviations. Fluctuations in signal were occasionally observed which required adjustment of the discriminator level. In these cases the experiment was repeated.

Once the optimum pressure for the Ar lamp was determined, the column was evacuated and background measurements were taken. For an experiment, where the data consisted of a series of scans, backgrounds were measured by comparing the observations to three spectra: the first with the fluorescence cell evacuated (i.e. lamp reflectance only), secondly, a scan with argon, and thirdly with hydrogen in the cell. In the latter two cases, trace impurities of the order of < 10ppm were assumed.

Mixing of the H_2 and Ar was usually carried out twenty-four hours before beginning an experiment. The technique used in mixing the gases consisted of evacuating the storage volume, fluorescence cell and connecting tubing followed by admitting the reagent gas to an accurately measured pressure. The hydrogen was then

diluted with Argon which was continuously admitted to the system, divided into two flows, under a continuous positive pressure of > 101.3 kPa.

Initially scans or count rates were taken using flowing mixtures. In this procedure the backing pressure was found to vary by as much as 50% due to the long duration of the experiment and a constant proportion of hydrogen was difficult to maintain. In later experiments a premixed quantity of H_2/Ar was allowed to flow through the fluorescence cell while monitoring the emission produced. In this case, pressures were limited (maximum 400Pa) and depletion of the mixture resulted in only one or two runs being carried out for an experiment. An experiment usually contained 9 to 14 runs. These two methods resulted in limited systematic runs that could be carried out for a given mixture during an experiment.

Identical results of sensitized emission were observed for the case of a static system. In this case the column and fluorescence cell were evacuated and a small amount of Ar/H_2 mixture was admitted to the cell and a run undertaken. At the completion of this run a larger amount of the same mixture was admitted to a higher total pressure and another run completed. In this method a pressure range from 1Pa to 6.65 kPa could be undertaken using a constant mixture of Argon and Hydrogen for a series of runs in an experiment.

Between runs, the fluorescence cell and column

were evacuated and background levels of the lamp and Lyman - α were monitored. This (static) method of experiments was found to be ideal because of the constant pressures observed for a run and the wide range of pressures that could be studied during an experiment.

During an experiment all conditions were kept constant except for total pressure which was varied from run to run. Slit widths of the monochromator were set between 50μ and 1mm and the Argon lamp power was intentionally kept at a minimum of approximately 17 Watts in order to keep colour centre formation of the lithium fluoride windows to a minimum. Conditions were varied between experiments in order to maximize observation of sensitized fluorescence of the Lyman bands.

The Argon used was standard grade Ar obtained from Liquid Carbonic, the Hydrogen was Ultra Pure grade and supplied by Gas Dynamics, 720 Progress Ave., Scarborough, Ont. M1H 2X3.

All the Lyman bands observed in the $v''(v' \approx 3)$ progression were studied.

c) SENSITIVITY OF THE DETECTION SYSTEM

Relative intensity measurements of the Lyman bands observed were studied to determine the relative sensitivity of the monochromator-detector apparatus in the wavelength range from 105.0 - 165.0 nm. The technique was similar to that proposed by McConkey (56);

FIG. 6. Relative sensitivity of the detecting system from 105 to 160 nm.
(See Appendix B for 1st order low resolution data in Table 6, 0 ; High resolution data normalized to R(0) branch from Table 7(a), + ; and P(2) branch from Table 7(b), X .)

FIG. 6. Relative sensitivity of the detecting system from 105 to 160 nm.
(See Appendix B for 1st order low resolution data in Table 6, **O** ; High resolution data normalized to R(0) branch from Table 7(a), **+** ; and P(2) branch from Table 7(b), **X** .)

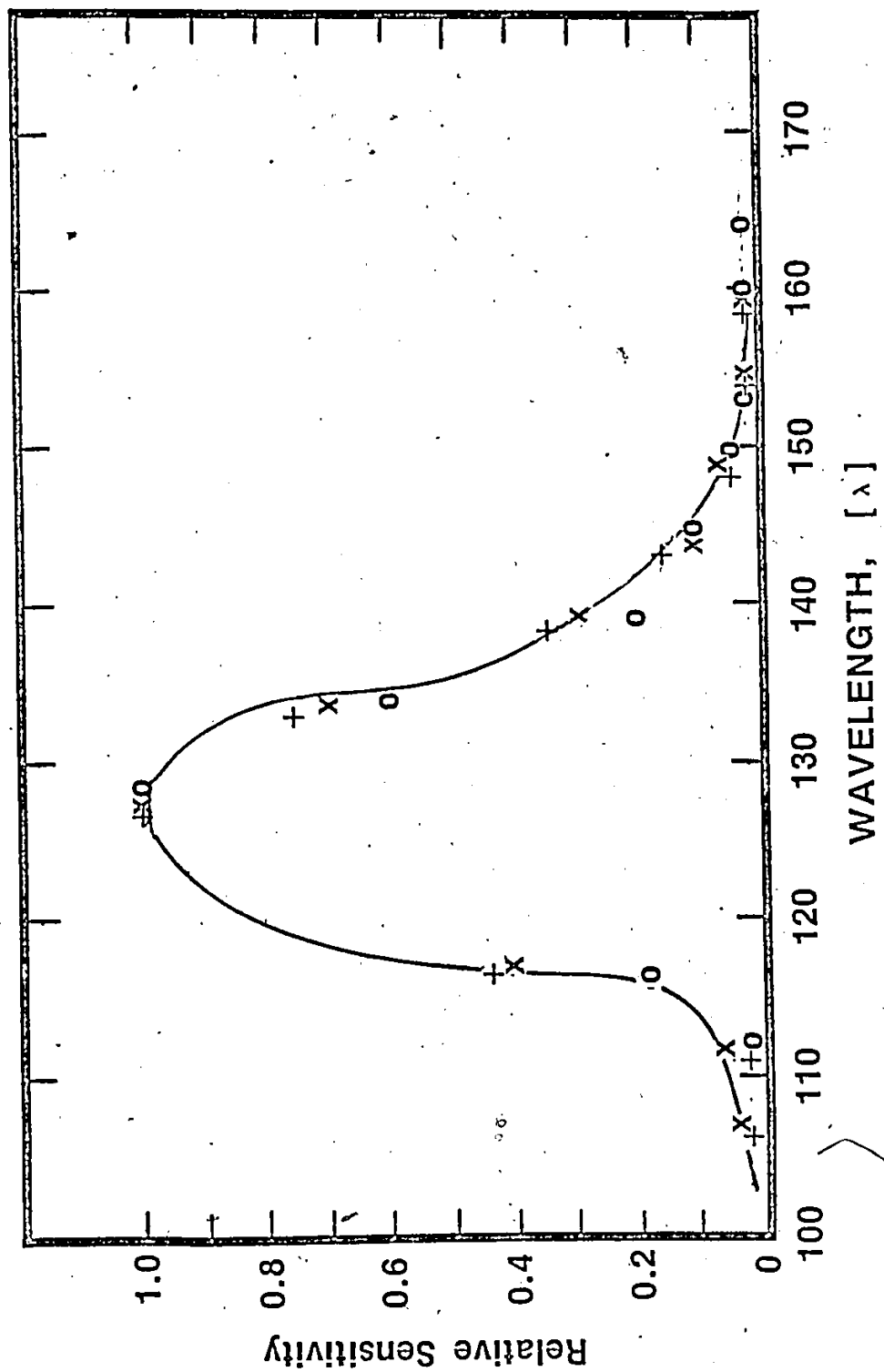


Fig. 6.
Relative Sensitivity of the Detecting System

which is similar to the branching-ratio technique using relative intensities of the lines observed and their corresponding transition probabilities. The calibration was performed to determine the optimum wavelength region for measurements of the sensitized fluorescence observed. A more complete description of this technique is given in the appendix, and Fig. 6 shows the final result as a plot of relative sensitivity as a function of wavelength. It can be seen that the detection system is most sensitive at wavelengths near the $v'=3, v''=4$ transition.

RESULTS

a) OVERALL OBSERVATIONS

Most of the available vibrational levels in the ground state or in the electronically excited state of a diatomic molecule are populated by an energy transfer mechanism (33), (53). Excitation of the $B^1\Sigma_u^+$ state of hydrogen is known to be populated by collisions of optically excited argon atoms with H_2 molecules (33), thus transferring electronic energy from Argon to Hydrogen accompanied by emission from the Lyman bands. Figs. 7(a) and 7(b) are schematic energy level diagrams describing the transitions observed for the Lyman bands.

Similar behaviour was observed for all bands of the $B^1\Sigma_u^+ \rightarrow X^1\Sigma_g^+$ transition. Fig. 8 shows how the

FIG. 7. (a) Transitions between the rotational-vibrational energy levels for the (3,4) band.. (Schematic)

(b) Pumping of the $v'=3, v''$ level of the $B^1\Sigma_u^+$ state of H_2 by Ar* excited by 106.6 nm radiation. The $v'=3, v''$ progression is emitted as sensitized fluorescence.

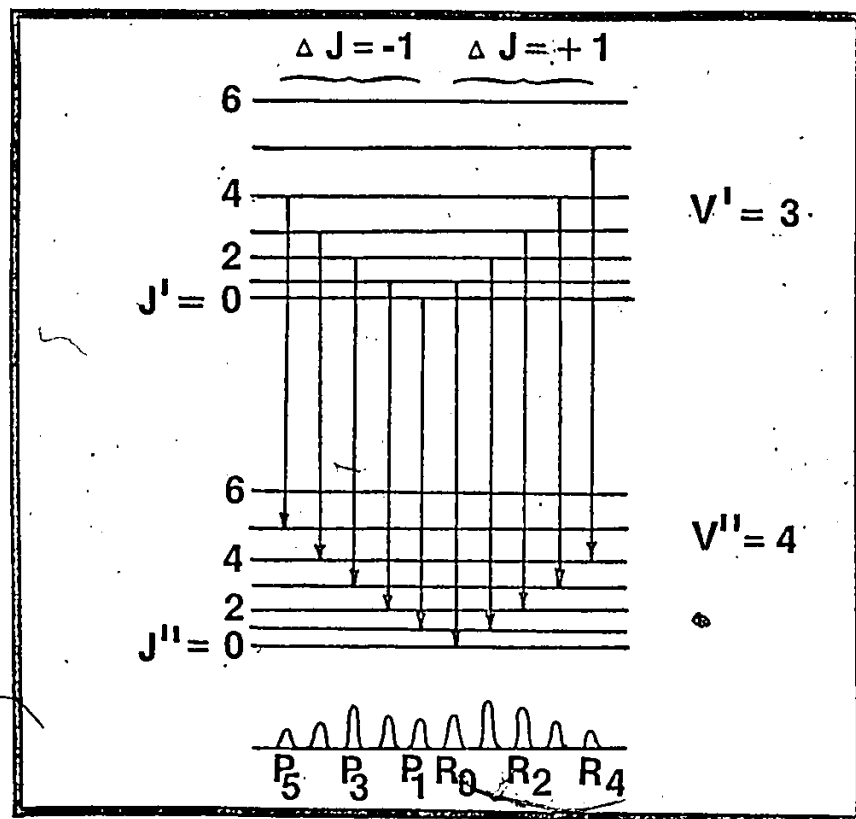


Fig. 7[a].
Schematic Energy Levels Diagram

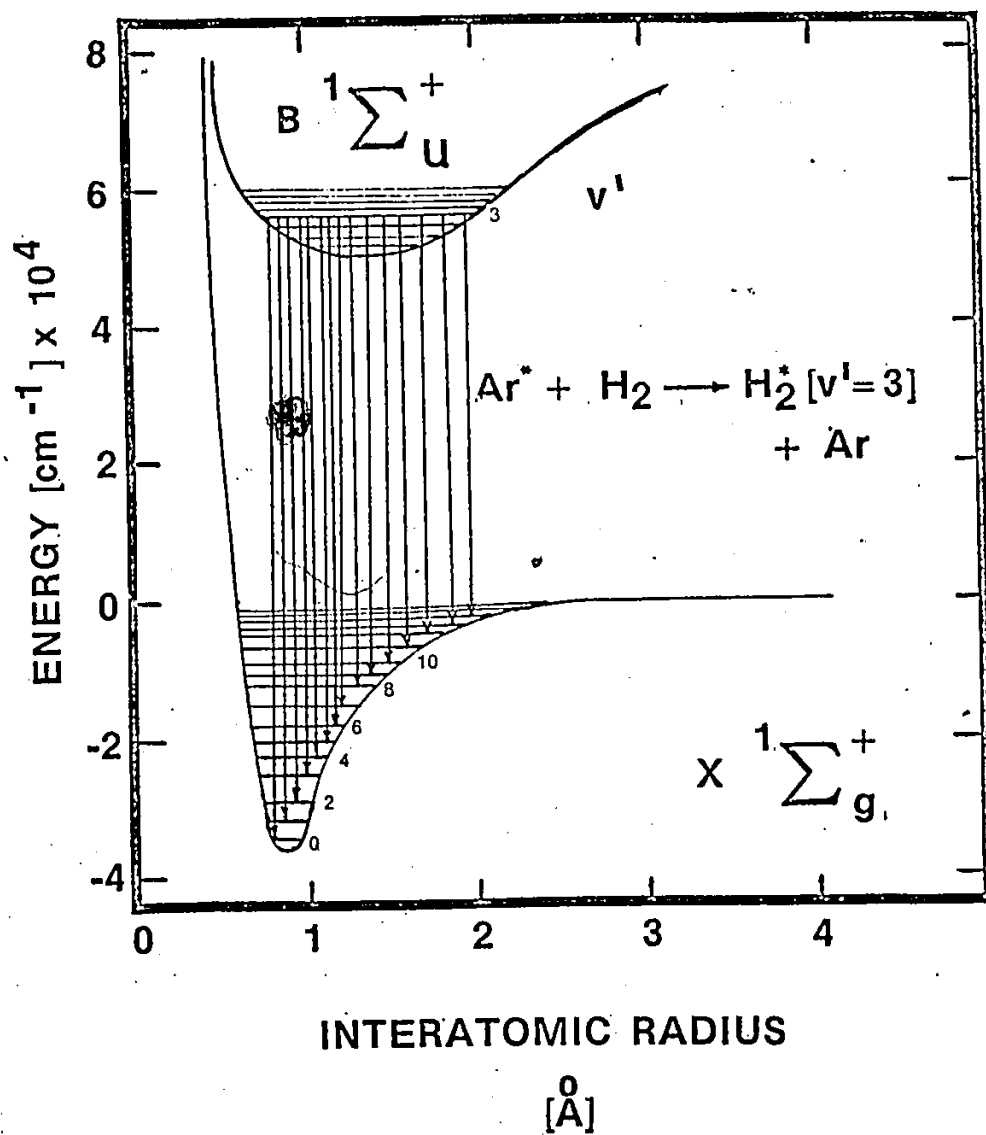


Fig. 7B.
Schematic Energy Level Diagram

FIG. 8. Plots of sensitized fluorescence corresponding to the R(0) branch, (3,4) band of the H_2^{\pm} ($B^1\Sigma_u^+ \rightarrow X^1\Sigma_g^+$) transition in low resolution studies. Approximate linearity is shown up to $P_{H_2} = 12$ Pa and a decrease in intensity is shown above pressures of 50 Pa. Abscissa scale change indicates behaviour of fluorescence intensity at very high pressures of hydrogen with trace impurities of argon ($\approx < 10$ ppm); \times (3,4); \circ (3,0); \square (3,1); \odot (3,2); \bullet (3,5).

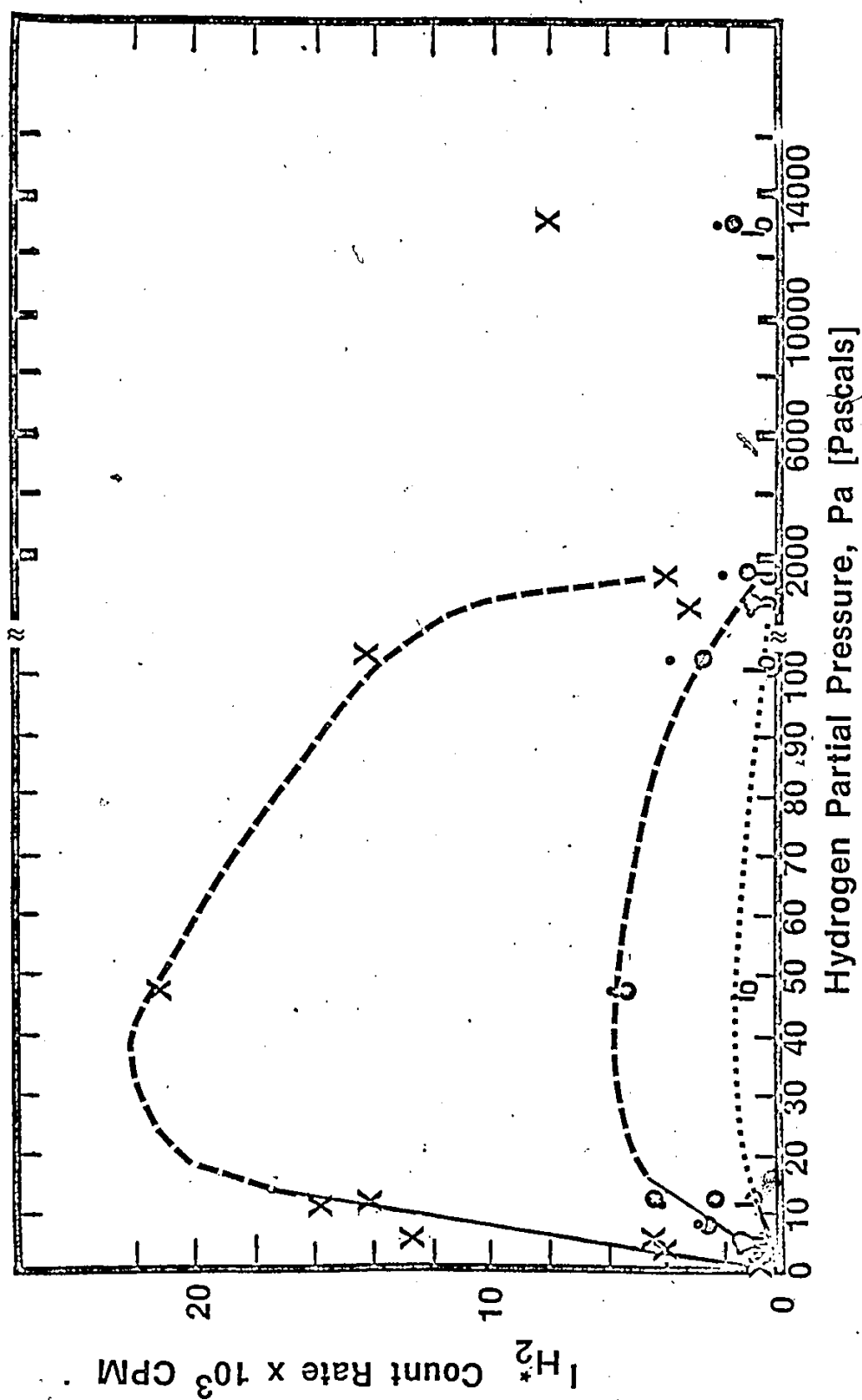


Fig. 8. Plots of Sensitized Fluorescence Intensity

intensity of the bands observed vary with pressure at low partial pressures of hydrogen. The intensities shown have not been corrected for the sensitivity of the detecting system.

Table 4 lists the counting rates for the low resolution data and the pressure range studied for one experiment.

Plots of the intensity of the H_2 sensitized fluorescence over the pressure range studied show a general increase over the region of low partial pressures of hydrogen used, followed by a general decrease in intensity, indicative of quenching. At very high partial pressures of hydrogen, the data points tend to scatter and remain approximately constant in intensity. The behaviour of the (3,4) band is indicated in Fig. 8.

Fig. 9 shows a complete spectrum of sensitized resonance fluorescence observed under conditions of low resolution when slit widths were 500μ . Interference from third order is also shown in Fig. 9. The (3,4) to (3,8) bands are the first in the progression to be free from the effects of overlap from the third order progression. The (3,5) to (3,8) bands were found to be of very weak intensity and in the less sensitive region of the detector response hence the (3,4) band is most representative of the $B \rightarrow X$ fluorescence.

Similar observations were noted for the high resolution spectra except that peaks arising from

Table 4. Experimental count rates observed for bands of sensitized fluorescence emission from H_2^+ ($B \ ^1\Sigma_u^+ \rightarrow X \ ^1\Sigma_g^+$) .
 Low resolution experiments. Mole percent of Hydrogen : 0.77%. Signal values were taken as photon counts integrated over 60 second intervals.

Notes from Table:

- (a) Count rate corresponds to R(0) branch
- (b) Count rate recorded immediately after R(0) value taken, corrected for background
- (c) Count rate corresponds to P(2) branch
- (d) Count rate recorded immediately after P(2) value taken, corrected for background
- (e) Fluorescence cell evacuated i.e. $P = 0$
- (f) Assumed Ar impurity level 10ppm i.e. studies using high partial pressures of Hydrogen.
- (g) Assumed H_2 impurity level.

TABLE 4
(3,4) BAND

Fluorescence Cell pressure Pa	Hydrogen partial pressure Pa	I _{R(0)} (a) λ = 507.4nm	I _{L-α} (b) λ = 486.3	I _{R(0)} (c) λ = 509.2 nm	I _{L-α} (d) λ = 486.3	I _{P(2)} (e) λ = 486.3
9.52 x 10 ²	7.32	12754	1358	9.39	1200	8.32
5.20 x 10 ²	4.00 x 10 ⁻¹	347	---	---	---	---
8.32 x 10 ²	6.39 x 10 ⁻¹	261	---	---	---	---
4.89 x 10 ²	3.76	4678	533	8.78	396	11.73
4.89 x 10 ²	3.76	4796	512	9.37	451	10.83
1.59 x 10 ³	1.22 x 10	14142	1465	9.65	1339	8.85
1.54 x 10 ³	1.18 x 10	15976	1808	8.84	1808	7.16
6.13 x 10 ³	4.72 x 10	21493	2556	8.41	2407	8.93
1.33 x 10 ⁴	1.02 x 10 ²	13651	1838	7.43	1802	5.50
0.00 (e)	0.00 (e)	140	0	---	0	---
5.56 x 10 ²	5.56 x 10 ² (f)	3144	426	7.38	426	13.6
1.58 x 10 ³	1.58 x 10 ³ (f)	4408	581	7.59	581	13.3
1.37 x 10 ⁴	1.37 x 10 ⁴ (f)	8200	966	8.49	1074	13.6
5.20 x 10 ²	10 ppm (g)	645	50	12.9	47	9.55
1.55 x 10 ³	10 ppm (g)	278	56	4.96	56	5.07
1.34 x 10 ⁴	10 ppm (g)	1510	1054	1.43	981	1.29

TABLE 4
(3,0) BAND

Fluorescence Cell pressure Pa	Hydrogen partial pressure Pa	(a) $I_R(0)$ $\lambda = 425.1 \text{ nm}$	(b) $I_{L-\alpha}$ $\lambda = 486.3$	$\frac{I_R(0)}{I_{L-\alpha}}$	(c) $I_P(2)$ $\lambda = 426.6 \text{ nm}$	(d) $I_{L-\alpha}$ $\lambda = 486.3$	$\frac{I_P(2)}{I_{L-\alpha}}$
9.52×10^2	7.32	471	3128	.1506	848	3012	.2815
5.20×10	4.00×10^{-1}	---	---	---	---	---	---
8.32×10	6.39×10^{-1}	---	---	---	---	---	---
4.89×10^2	3.76	115	1202	.0957	325	1111	.2925
4.89×10^2	3.76	---	---	---	---	---	---
1.59×10^3	1.22×10	409	2853	.1434	667	2274	.2933
1.54×10^3	1.18×10	---	---	---	---	---	---
6.13×10^3	4.72×10	422	2852	.1480	552	2669	.2068
1.33×10^4	1.02×10^2	252	1968	.1280	356	2083	.1709
0.00 (e)	0.00 (e)	---	0	---	0	0	---
5.56×10^2	5.56×10^2 (f)	0	412	---	18	400	.0450
1.58×10^3	1.58×10^3 (f)	19	470	.0404	35	485	.0722
1.37×10^4	1.37×10^4 (f)	62	980	.0633	135	963	.1400
5.20×10^2	10 ppm (g)	0	67	.0000	180	21	8.58
1.55×10^3	10 ppm (g)	0	126	.0000	260	92	2.83
1.34×10^4	10 ppm (g)	291	3704	.0786	297	3561	.0834

TABLE 4
(31) BAND

Fluorescence Cell pressure Pa	Hydrogen partial pressure Pa	I _R (0) λ=444.8 nm	I _{L-α} λ=486.3	I _R (0) I _{L-α}	I _P (2) λ=446.5 nm	I _{L-α} λ=486.3	I _P (2) I _{L-α}
9.52 x 10 ²	7.32	558	2136	.2612	1716	1930	.8891
5.20 x 10 ²	4.00 x 10 ⁻¹	---	---	---	---	---	---
8.32 x 10 ²	6.39 x 10 ⁻¹	---	---	---	---	---	---
4.89 x 10 ²	3.76	133	855	.1556	664	733	.8786
4.89 x 10 ²	3.76	---	---	---	---	---	---
1.59 x 10 ³	1.22 x 10	513	2145	.2392	1844	2043	.9026
1.54 x 10 ³	1.18 x 10	---	---	---	---	---	---
6.13 x 10 ³	4.72 x 10	598	2777	.2153	2198	3117	.7052
1.33 x 10 ⁴	1.02 x 10 ²	434	2130	.2038	1234	2020	.6109
0.00 (e)	0.00 (e)	0	0	---	0	0	---
5.56 x 10 ²	5.56 x 10 ² (f)	43	426	.1010	272	529	.5140
1.58 x 10 ³	1.58 x 10 ³ (f)	61	581	.1050	377	629	.5990
1.37 x 10 ⁴	1.37 x 10 ⁴ (f)	224	1009	.2220	824	965	.8540
5.20 x 10 ²	10 ppm (g)	0	54	0	180	21	8.57
1.55 x 10 ³	10 ppm (g)	20	56	.3570	0	47	0.0
1.34 x 10 ⁴	10 ppm (g)	108	3112	.0347	117	2119	.0552

TABLE 4
(3,2) BAND

Fluorescence Cell pressure Pa	Hydrogen partial pressure Pa	I _R (0) λ=465.1 nm	I _{L-α} λ= 486.3	I _R (0) I _{L-α}	I _P (2) λ=466.8 nm	I _{L-α} λ=486.3	I _P (2) I _{L-α}
9.52 x 10 ²	7.32	3667	1809	2.03	2694	1637	1.65
5.20 x 10	4.00 x 10 ⁻¹	----	----	----	----	----	----
8.32 x 10	6.39 x 10 ⁻¹	----	----	----	----	----	----
4.89 x 10 ²	3.76	1248	695	1.80	1080	636	1.70
4.89 x 10 ²	3.76	1363	813	1.68	1048	574	1.83
1.59 x 10 ³	1.22 x 10	2082	935	2.23	3094	1854	1.67
1.54 x 10 ³	1.18 x 10	4362	2387	1.83	3300	2387	1.38
6.13 x 10 ³	4.72 x 10	5597	3020	1.85	4020	2921	1.38
1.33 x 10 ⁴	1.02 x 10 ²	3372	2036	1.66	2345	1964	1.19
0.00 (e)	0.00 (e)	0	0	----	0	0	----
5.56 x 10 ²	5.56 x 10 ² (f)	647	426	1.52	1120	426	2.63
1.58 x 10 ³	1.58 x 10 ³ (f)	905	645	1.40	1371	581	2.36
1.37 x 10 ⁴	1.37 x 10 ⁴ (f)	1616	1009	1.60	2726	1059	2.57
5.20 x 10 ²	10 ppm (g)	27	54	0.50	59	63	.937
1.55 x 10 ³	10 ppm (g)	1	56	0.018	0	24	0.00
1.34 x 10 ⁴	10 ppm (g)	555	1795	0.309	521	1384	0.376

TABLE 4
(3,3) BAND

Fluorescence Cell pressure Pa	Hydrogen partial pressure Pa	$I_R(0)$ $\lambda=486.0$ nm	$I_{L-\alpha}^{(b)}$ $\lambda=486.3$ nm	$\frac{I_R(0)}{I_{L-\alpha}}$	$I_P(2)$ $\lambda=487.8$ nm	$I_{L-\alpha}^{(d)}$ $\lambda=486.3$ nm	$\frac{I_P(2)}{I_{L-\alpha}}$
9.52×10^2	7.32	1684	1561	1.08	1610	1435	1.12
5.20×10	4.00×10^{-1}	---	---	---	---	---	---
8.32×10	6.39×10^{-1}	---	---	---	---	---	---
4.89×10^2	3.76	797	587	1.36	739	508	1.45
4.89×10^2	3.76	---	---	---	---	---	---
1.59×10^3	1.22×10	---	---	---	---	---	---
1.54×10^3	1.18×10	1834	1596	1.15	1779	1527	1.17
6.13×10^3	4.72×10	2811	2777	1.01	2479	2762	0.898
1.33×10^4	1.02×10^2	1975	1890	1.05	1772	1859	0.953
0.00 (e)	0.00 (e)	0	0	---	0	0	---
5.56×10^2	5.56×10^2 (f)	533	447	1.19	757	378	2.00
1.58×10^3	1.58×10^3 (f)	796	581	1.37	1114	580	1.92
1.37×10^4	1.37×10^4 (f)	1181	1046	1.13	1961	1082	1.81
5.20×10^2	10 ppm (g)	204	50	4.08	92	27	3.41
1.55×10^3	10 ppm (g)	234	56	4.18	48	72	0.667
1.34×10^4	10 ppm (g)	1402	1415	0.991	1311	1077	1.22

TABLE 4
(3,5) BAND

Fluorescence Cell pressure Pa	Hydrogen partial pressure Pa	I _R (0) λ=529.1 nm	I _{L-α} λ= 486.3	I _R (0) I _{L-α}	I _P (2) λ=531.0 nm	I _{L-α} λ=486.3	I _P (2) I _{L-α}
9.52 x 10 ²	7.32	3366	1308	2.57	2432	1170	2.08
5.20 x 10	4.00 x 10 ⁻¹	----	----	----	----	----	----
8.32 x 10	6.39 x 10 ⁻¹	----	----	----	----	----	----
4.89 x 10 ²	3.76	1134	336	3.38	916	314	2.92
4.89 x 10 ²	3.76	----	----	----	----	----	----
1.59 x 10 ³	1.22 x 10	----	----	----	----	----	----
1.54 x 10 ³	1.18 x 10	4098	1387	2.95	2728	1366	1.99
6.13 x 10 ³	4.72 x 10	6014	2198	2.74	3234	2205	1.47
1.33 x 10 ⁴	1.02 x 10 ²	4201	1826	2.30	2331	1823	1.29
0.00 (e)	0.00 (e)	0	0	----	0	0	----
5.56 x 10 ²	5.56 x 10 ² (f)	909	555	1.64	1454	454	3.20
1.58 x 10 ³	1.58 x 10 ³ (f)	1196	581	2.06	1935	580	3.34
1.37 x 10 ⁴	1.37 x 10 ⁴ (f)	2497	1059	2.36	3636	1059	3.43
5.20 x 10 ²	10 ppm (g)	163	21	7.76	118	19	6.21
1.55 x 10 ³	10 ppm (g)	31	56	.553	25	56	.446
1.34 x 10 ⁴	10 ppm (g)	356	954	.373	245	812	.302

TABLE 4
(3,6) BAND

Fluorescence Cell pressure Pa	Hydrogen partial pressure Pa	I _R (a) λ= 551.1nm	I _{L-α} (b) λ= 486.3	I _R (0) I _{L-α}	I _P (c) λ= 553.0nm	I _{L-α} (d) λ=486.3	I _P (2) I _{L-α}
9.52 x 10 ²	7.32	608	1132	0.537	656	1071	0.612
5.20 x 10	4.00 x 10 ⁻¹	---	---	---	---	---	---
8.32 x 10	6.39 x 10 ⁻¹	---	---	---	---	---	---
4.89 x 10 ²	3.76	119	298	0.399	183	236	0.775
4.89 x 10 ²	3.76	160	415	0.400	254	390	0.651
1.59 x 10 ³	1.22 x 10	747	1203	0.621	766	1157	0.662
1.54 x 10 ³	1.18 x 10	915	1512	0.605	850	1670	0.509
6.13 x 10 ³	4.72 x 10	1251	2309	0.542	1021	2350	0.435
1.33 x 10 ⁴	1.02 x 10 ²	871	1811	0.481	761	1795	0.424
0.00 (e)	0.00 (e)	0	0	---	0	0	---
5.56 x 10 ²	5.56 x 10 ² (f)	165	426	0.387	362	426	0.850
1.58 x 10 ³	1.58 x 10 ³ (f)	200	581	0.344	491	581	0.845
1.37 x 10 ⁴	1.37 x 10 ⁴ (f)	467	1059	0.441	1076	1059	1.020
5.20 x 10 ²	10 ppm (g)	0	54	0.000	0	47	0.000
1.55 x 10 ³	10 ppm (g)	0	56	0.000	0	46	0.000
1.34 x 10 ⁴	10 ppm (g)	41	754	0.054	1	705	0.001

TABLE 4
(3,7) BAND

Fluorescence Cell pressure Pa	Hydrogen partial pressure Pa	I _R (0) λ=573.1 nm	I _{L-α} λ=486.3	I _R (0) I _{L-α}	I _P (2) λ=575.0 nm	I _{L-α} λ=486.3	I _P (2) I _{L-α}
9.52 x 10 ²	7.32	1604	1114	1.44	1378	1108	1.24
5.20 x 10	4.00 x 10 ⁻¹	---	---	---	---	---	---
8.32 x 10	6.39 x 10 ⁻¹	---	---	---	---	---	---
4.89 x 10 ²	3.76	420	162	2.59	423	225	1.88
4.89 x 10 ²	3.76	---	---	---	---	---	---
1.59 x 10 ³	1.22 x 10	---	---	---	---	---	---
1.54 x 10 ³	1.18 x 10	1820	1172	1.55	1414	1105	1.28
6.43 x 10 ³	4.72 x 10	3185	2395	1.33	2099	2502	0.839
1.33 x 10 ⁴	1.02 x 10 ²	2234	1851	1.21	1388	1634	0.849
0.00 (e)	0.00 (e)	0	0	---	0	0	---
5.56 x 10 ²	5.56 x 10 ² (f)	527	426	1.24	1117	426	2.62
1.58 x 10 ³	1.58 x 10 ³ (f)	720	581	1.24	1572	581	2.71
1.37 x 10 ⁴	1.37 x 10 ⁴ (f)	1413	1059	1.33	2598	1100	2.36
5.20 x 10 ²	10 ppm (g)	14	54	.259	63	47	1.34
1.55 x 10 ³	10 ppm (g)	0	56	0.00	0	56	0.00
1.34 x 10 ⁴	10 ppm (g)	12	679	0.018	4	661	0.006

FIG. 9. Low resolution sensitized resonance fluorescence spectrum of H_2^* . One major progression is observed from $v'=3$ in two orders (3rd and 4th). Partial pressure of $H_2 = 97.3$ Pa at a total pressure of 479 Pa. Slits were set at 500 microns and scan rate 1.0 nm min^{-1} .

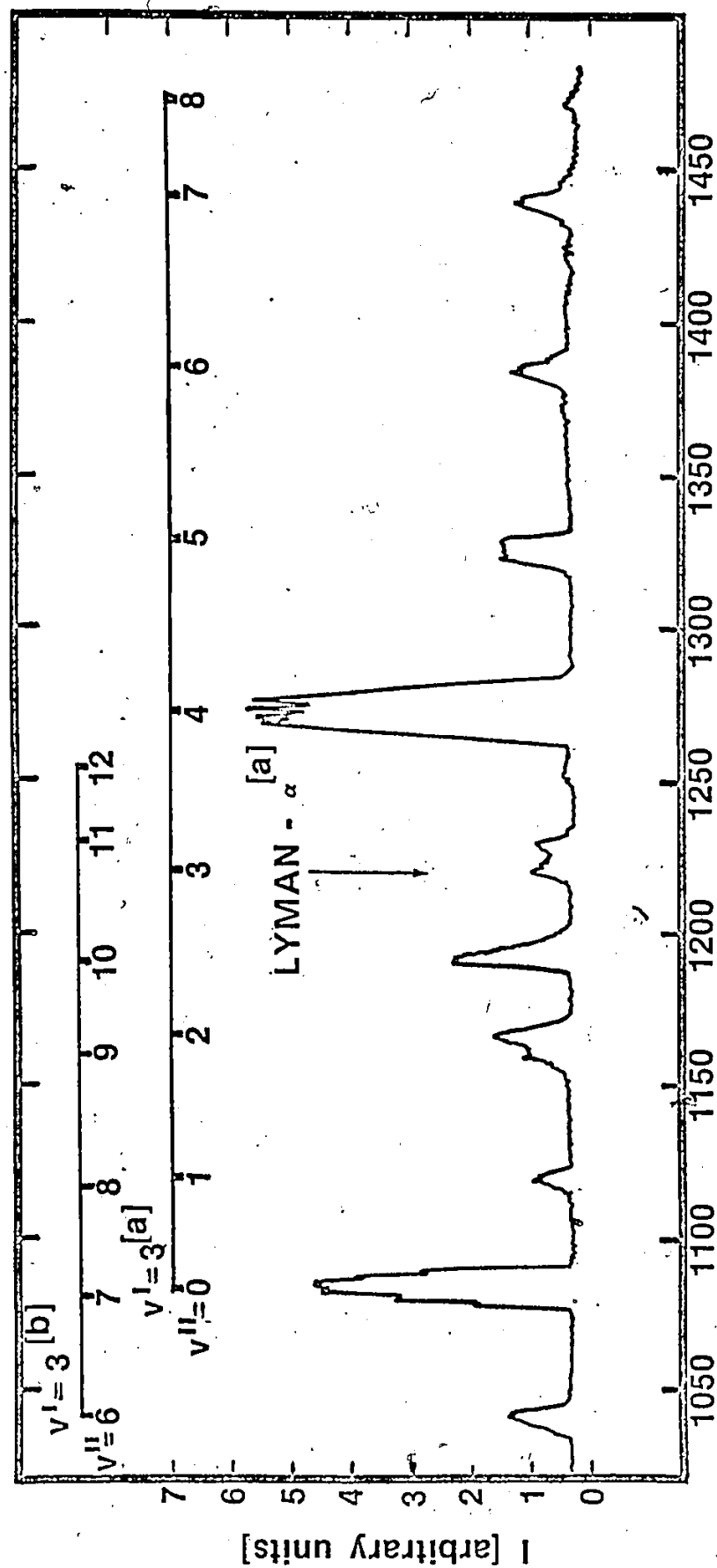


Fig. 9.
 Low Resolution Sensitized Resonance Fluorescence Spectrum of H₂
 [a] 4th Order [b] 3rd Order

$J' = 0 - 4$ rotational levels could be seen with the $[P(1), R(2)]$, $[R(0), R(1)]$, and $[P(2), R(3)]$ pairs unresolved

A typical tracing of a $v'=3$, $v''=4$ resolved band is shown in Fig. 10. The upper portion is under conditions of low partial pressure of H_2 and the lower tracing shows the effect of high hydrogen partial pressures while all other conditions remained constant.

At high H_2 concentrations the unresolved pairs $[R(0), P(1)]$ and $[P(2), R(3)]$ are the only significant fluorescence peaks observed. The reason for this is due to the bulk of the population being in the $J' = 0, 1$ levels, probably as a result of rapid rotational-rotational quenching collisions.

b) INTERPRETATION OF RESULTS - LOW RESOLUTION STUDIES

The results show fluorescence emission of the H_2 Lyman bands sensitized by argon. There is a general increase in intensity with increasing pressures and a quenching process at higher pressures (see Fig. 8). The overall observations follow a regular behaviour over the conditions studied and may be used to suggest a possible mechanism for the reactions observed.

c) KINETIC ANALYSIS

The relative fluorescence intensities should be directly related to the relative rates of sensitized excitation of the hydrogen ($v' J'$) levels by Argon, (33). Since B state hydrogen radiates with a lifetime of

FIG. 10. High resolution sensitized resonance fluorescence scans of low (upper tracing) and high (lower tracing) partial pressures of Hydrogen. The Argon lamp was maintained at a power of 25 W at a pressure of 219 Pa. The partial pressure of Hydrogen in the upper tracing was 507 Pa at a total pressure of 4000 Pa. In the lower tracing the partial pressure of H_2 was essentially the same as the total pressure of 4467 Pa. A small amount of Ar Impurity is assumed in the lower tracing ($< 1\%$).

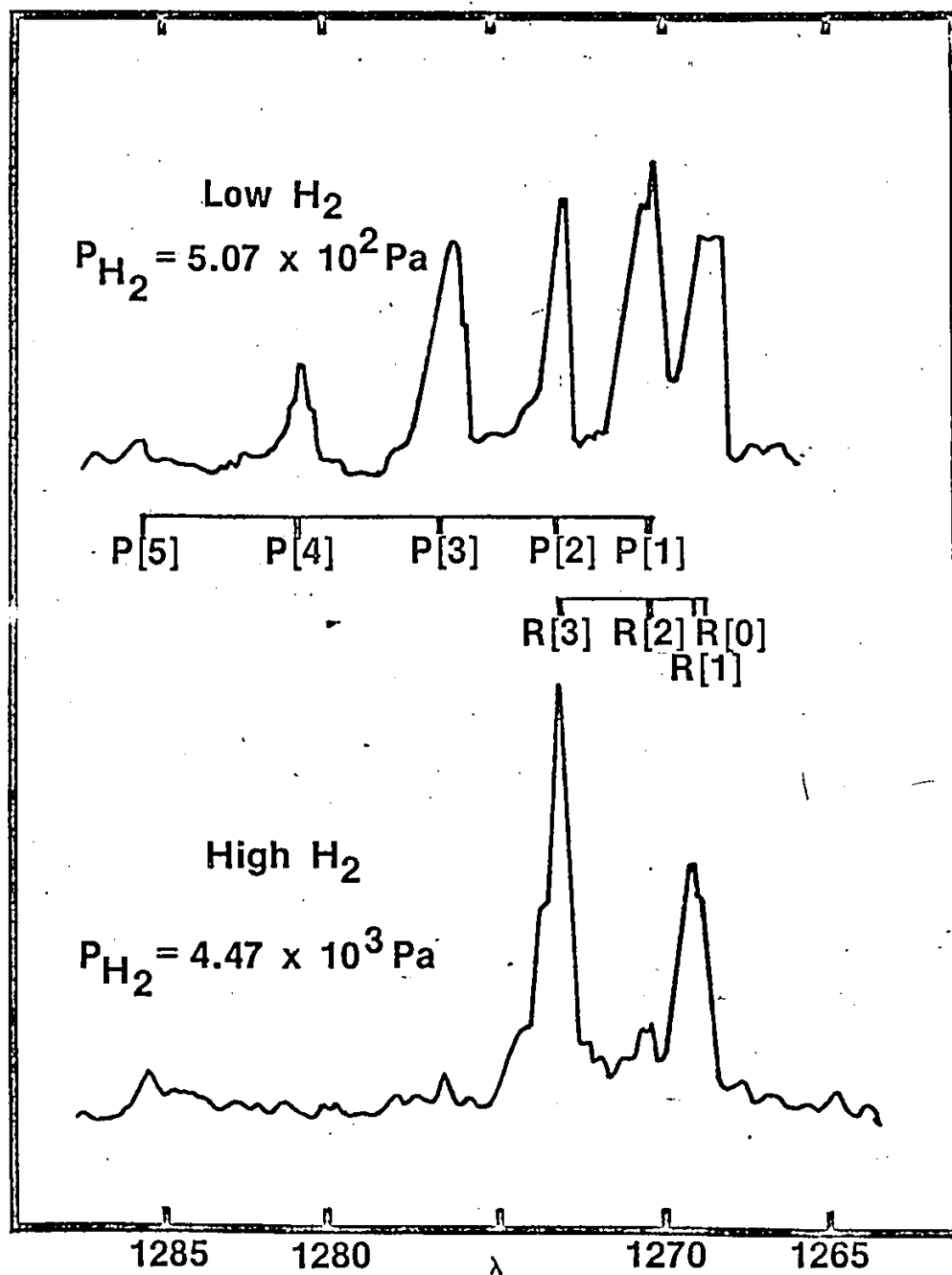
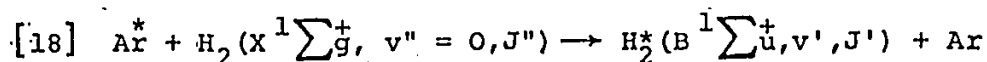


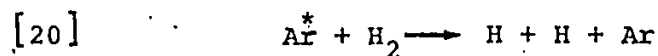
Fig. 10.

High Resolution Sensitized Resonance
 Fluorescence Scans of Low and High
 Partial Pressures of Hydrogen

approximately 6×10^{-10} sec, the fluorescence spectrum over the pressure region studied should give the rate constant for the following process:



A kinetic scheme of the reactions occurring in the system under study is proposed as below. The rate constants k are actually $\sum_{i=0}^J k_i$ (i.e. k_i are summed over all rotational states).



(i) Low Pressure

Application of steady state approximation yield the following:

$$\frac{d[\text{H}_2^*]}{dt} = k_{18}[\text{Ar}^*][\text{H}_2] - k_{19}[\text{H}_2^*] = 0$$

$$\text{hence} \quad [\text{H}_2^*] = \frac{k_{18}[\text{Ar}^*][\text{H}_2]}{k_{19}}$$

$$[25] \quad I_{\text{H}_2^*} = k_{19}[\text{H}_2^*] = k_{18}[\text{Ar}^*][\text{H}_2]$$

Equation [25] predicts that a plot of the H_2^* fluorescence intensity vs. the concentration of H_2 should give a straight line with a slope equal to $k_{18} [Ar^*]$. McNeely et al. (31) obtained a rate constant k_{18} of $1.26 \times 10^{14} \text{ cc mol}^{-1} \text{ s}^{-1}$ for $Ar(^3P_1)$ electronic energy exchange using a time resolved quenching technique. In this work, Fig. 8 shows a straight line is observed for partial pressures up to 12 Pa of H_2 for the $v''=3, v'=4$ band. Similar behaviour was observed for the other bands, however the scatter was much larger due to the low intensities observed.

$$\frac{d[H^*]}{dt} = k_{21} [H] - k_{22} [H^*] = 0$$

$$\text{and } k_{22} [H^*] = I_{L-\alpha} = k_{21} [H] = \frac{1}{I_{L-\alpha}} [H^*]$$

$$\frac{d[H]}{dt} = 2k_{20} [H_2] [Ar^*] - k_{21} [H] + k_{22} [H^*] - k_w [H] = 0$$

$$[26] \quad [H] = \frac{2k_{20} [Ar^*] [H_2]}{k_w}$$

$$I_{L-\alpha} = k_{22} [H^*] = k_{21} [H] = \frac{k_{21} 2k_{20} [Ar^*] [H_2]}{k_w}$$

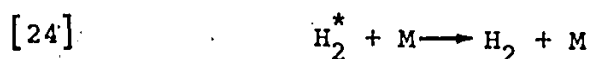
$$[27] \quad \frac{I_{H_2^*}}{I_{L-\alpha}} = \frac{k_w k_{18} [Ar^*] [H_2]}{k_{21} 2k_{20} [Ar^*] [H_2]} = \frac{1}{2} \frac{k_{18} k_w}{k_{20} k_{21}}$$

Equation [27] indicates that if a plot is made of the fluorescence intensity relative to that of atomic hydrogen fluorescence (Lyman- α) against the pressure of hydrogen, then a straight line should be observed parallel to the abscissa. This indicates that

$\frac{1}{2} \frac{k_{18} k_w}{k_{20} k_{21}} = \text{constant}$ and that there is a constant proportion of H atoms to H_2 which is essentially invariant for the pressure range studied. This supports the mechanism proposed for hydrogen atom production. Using the data from Table 4 we see that $\frac{I_{H_2^*}}{I_{L-\alpha}}$ remains approximately constant over the entire pressure range studied as shown in Fig. 11 for the (3,4) band.

(ii) High Pressure

An additional reaction must be considered for the case of high pressure:



In this case:

$$\frac{d[H_2^*]}{dt} = k_{18} [Ar^*] [H_2] - k_{19} [H_2^*] - k_{24} [H_2^*] [M] = 0$$

$$[H_2^*] = \frac{k_{18} [Ar^*] [H_2]}{k_{19} + k_{24} [M]}$$

$$[28] \quad I_{H_2^*} = k_{19} [H_2^*] = \frac{k_{18} k_{19} [Ar^*] [H_2]}{k_{19} + k_{24} [M]}$$

FIG. 11. Plot of resonant fluorescence intensity relative to atomic hydrogen fluorescence (Lyman- α) over a pressure range of 1 - 14000 Pa. The linear relationship supports equation [27], $I_{H_2^*} / I_{L-\alpha} = \text{const.}$

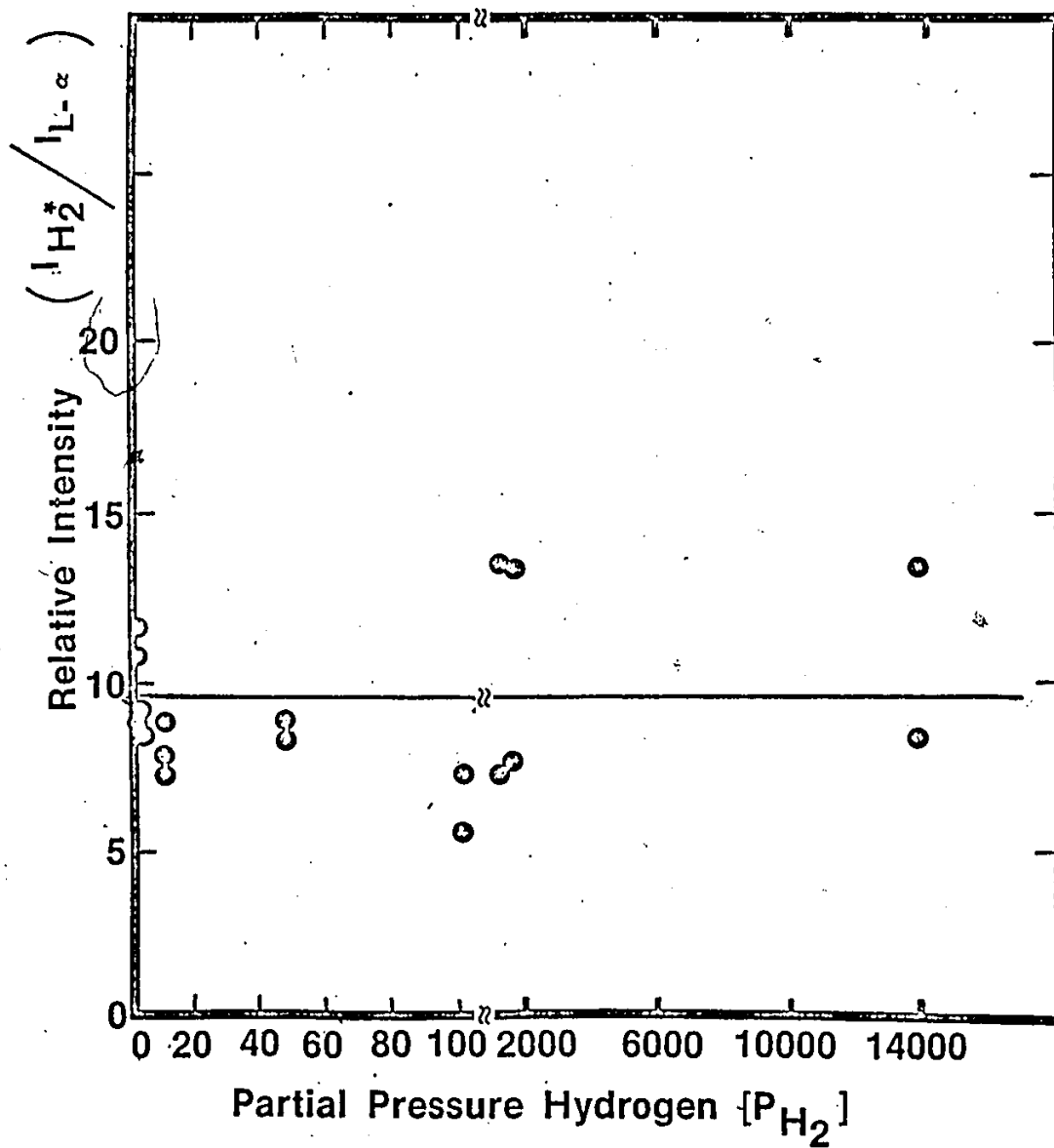


Fig. II.

Plot of Resonant Fluorescence Intensity Relative to Atomic Hydrogen Fluorescence

For the low pressure case $k_{19} \gg k_{24}$ and we would expect the intensity of the resonance fluorescence to increase with pressure as Fig. 8 indicates in the low pressure region. The fluorescence intensity starts to decrease at a H_2 partial pressure of ≈ 20 Pa. In this region $k_{19} \approx k_{24} [M]$ and above this pressure the dominant feature is $k_{24} [M]$ where equation [29] applies.

$$[29] \quad I_{H_2}^* = \frac{k_{18} k_{19} [Ar^*] [H_2]}{k_{24} [M]}$$

In the experiments carried out thus far it is difficult to determine which species is more important in quenching (H_2 or Ar) due to a lack of data. A more thorough procedure is required in order to accurately determine the quenching process. In this experiment quenching appears to start at about a partial pressure of hydrogen of about 50 Pa and at a total pressure of 6×10^3 Pa. If we assume that $k_{19} = k_Q [M]$ where $k_{19} = (H_2^* \text{ radiative lifetime})^{-1} = 1.67 \times 10^9 \text{ s}^{-1}$, and M is the quenching gas, then in the former case we have a concentration of H_2 as $n/v = 1.34 \times 10^{-5} \text{ mol cc}^{-1}$ from which $k_Q^{H_2} = k_{24}/[M] = 1.25 \times 10^{14} \text{ cc mol}^{-1} \text{ s}^{-1}$. For the latter case using the total pressure $k_Q^{Ar/H_2} = k_{24}/[M] = 9.61 \times 10^{11} \text{ cc mol}^{-1} \text{ s}^{-1}$.

Fink et al. (40) studied electronic fluorescence, quenching of HD and arrived at a value of 79 \AA^2

($k_Q^{HD} = 2.73 \times 10^{15} \text{ cc mol}^{-1} \text{ s}^{-1}$) for self-quenching.

The reciprocal of equation [28] gives the usual Stern-Volmer (50), (57) expression:

$$\begin{aligned}
 [30] \quad \frac{1}{I_f} &= \frac{1}{k_{18}[\text{Ar}^*]} \frac{k_{19} + k_{24} [M]}{k_{19} [\text{H}_2]} \\
 &= \frac{1}{k_{18} [\text{Ar}^*] [\text{H}_2]} + \frac{k_{24} [M]}{k_{18} k_{19} [\text{Ar}^*] [\text{H}_2]}
 \end{aligned}$$

A plot of $[\text{H}_2]/I_f$ against $[M]$ predicts a straight line with slope equal to $k_{24}/k_{18}k_{19}[\text{Ar}^*]$ and intercept of $1/k_{18}[\text{Ar}^*][\text{H}_2]$. The ratio of the slope to intercept is:

$$\begin{aligned}
 [31] \quad \{\text{slope/intercept}\} &= (k_{24}/k_{18}k_{19}[\text{Ar}^*]) / (1/k_{18}[\text{Ar}^*][\text{H}_2]) \\
 &= \frac{k_{24} [\text{H}_2]}{k_{19}}
 \end{aligned}$$

Plots were made using data from Table 4

($\frac{P_{\text{H}_2}}{I_{\text{H}_2}^*}$ vs. $[M]_{\text{H}_2}$), but resulted in large scatter and

a generally inconclusive relationship because of a lack of data in the quenching region under study.

d) PRODUCTION OF HYDROGEN ATOMS

Early experiments carried out in this laboratory indicated an enhancement of H production in H_2/Ar mixtures under various conditions. Sensitized emission from $v'=3, v''=3$ occurs at nearly the same wavelength

as Lyman- α , i.e., at 121.5 nm. Becker et al (58) cite the transition probability of the R(0) branch as $0.046 \times 10^8 \text{ sec}^{-1}$ and that of the P(2) branch (121.9 nm) as $0.125 \times 10^8 \text{ s}^{-1}$ which are proportioned to the intensity of the observed branches. In this experiment the P(2) branch of the (3,3) band was always less intense than Lyman- α by at least 50%, and from the transition probabilities it would be expected that the R(0) would be $\approx 30\%$ less than the P(2) branch, hence we would expect the contribution to Lyman- α by the R(0) branch not to exceed $\approx 15\%$.

H atoms are produced by reaction [20] of the mechanism given earlier. Fig. 11 shows a constant relationship between sensitized fluorescence and Lyman- α fluorescence, indicating support for the proposed mechanism.

From the mechanism, knowing the intensity of the Lyman- α radiation and the atomic concentration of hydrogen, we could arrive at a value of k_{20} for dissociation of H_2 in collision with Ar^* if we know the $[\text{Ar}^*]$ and the wall recombination rate constant k_w . In this case a plot of $[\text{H}]$ vs. $[\text{H}_2]$ gives a slope of $2k_{20} [\text{Ar}^*] / k_w$.

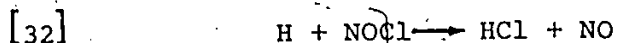
e) DETERMINATION OF H ATOM CONCENTRATION

Clyne and Stedman (59) pioneered a study of the reaction of H atoms with NOCl in the gas phase. They

found that the products were HCl and NO and that the stoichiometry of the reaction was close to 1:1 in a flow system with the walls poisoned with H_3PO_4 .

Reaction [32] was shown (59) to be very fast

$$(k_{32} = 1.5 \times 10^{-12} \text{ cm}^3 \text{ molecule}^{-1} \text{ sec}^{-1}).$$



M. Dunn et al. (60) re-investigated reaction [32] and found that 1:1 stoichiometry is preserved only when the walls of the reaction column are freshly poisoned to prevent the recombination of Chlorine atoms.

A gas phase titration was carried out using a fairly new phosphoric acid wall coating in order to determine an absolute value of $[H]$ corresponding to the approximate detector response observed in the fluorescence experiments. The concentration range studied was from 4×10^{-12} to 4×10^{-10} mols cc^{-1} . Extremely large scatter was observed in the data taken and a continual decay of background radiation was noted (from ≈ 2000 counts per minute at the beginning of the experiment to ≈ 500 counts per minute at the conclusion of the experiment).

The experiment was repeated with a new column and a fresh coating of "Siliclad" purchased from Clay Adams, Parsippany, New Jersey, USA. Siliclad is a water soluble silicone concentrate of a semi-organic nature that is characterized by a high degree of stability. In previous experiments we found that Siliclad helped reduce the

heterogeneous recombination of Hydrogen atoms in a fast flow apparatus.

Titration were carried out again over a concentration range from 1×10^{-13} to 9×10^{-12} moles cc^{-1} .

Considerable scatter was again observed, however the data fell into more or less a straight line.

(see Fig. 12) Lyman- α intensities were obtained by subtracting the background observed at each measurement. From this plot a correlation of Lyman- α intensity and $[\text{H}]$ atom concentration may be estimated.

A low resolution spectrum carried out immediately after the $[\text{H}]$ atom calibration indicated an intensity corresponding to a concentration of $\approx 1 \times 10^{11}$ atoms/cc.

In order to obtain a value of k_{20} for dissociation of H_2 , a series of experiments need to be undertaken at various H_2 concentrations and the absolute value of $[\text{H}]$ determined for each run. Upon determination of the wall recombination rate k_w , and using equation [26] a value of $k_{20} [\text{Ar}^*]$ could be obtained.

Previous results such as those listed in Table 4 could not be used for a reliable estimation of $[\text{H}]$ due to the constant decrease of Lyman- α fluorescence that was observed because of rapid decay of LiF transmission. Fig. 13 illustrates a typical decay plot. The reason for the decay has been attributed to colour centre formation of the LiF windows and atom recombination in the reactor.

FIG. 12. Calibration curve used in
determination of Absolute
concentration of atomic
Hydrogen.

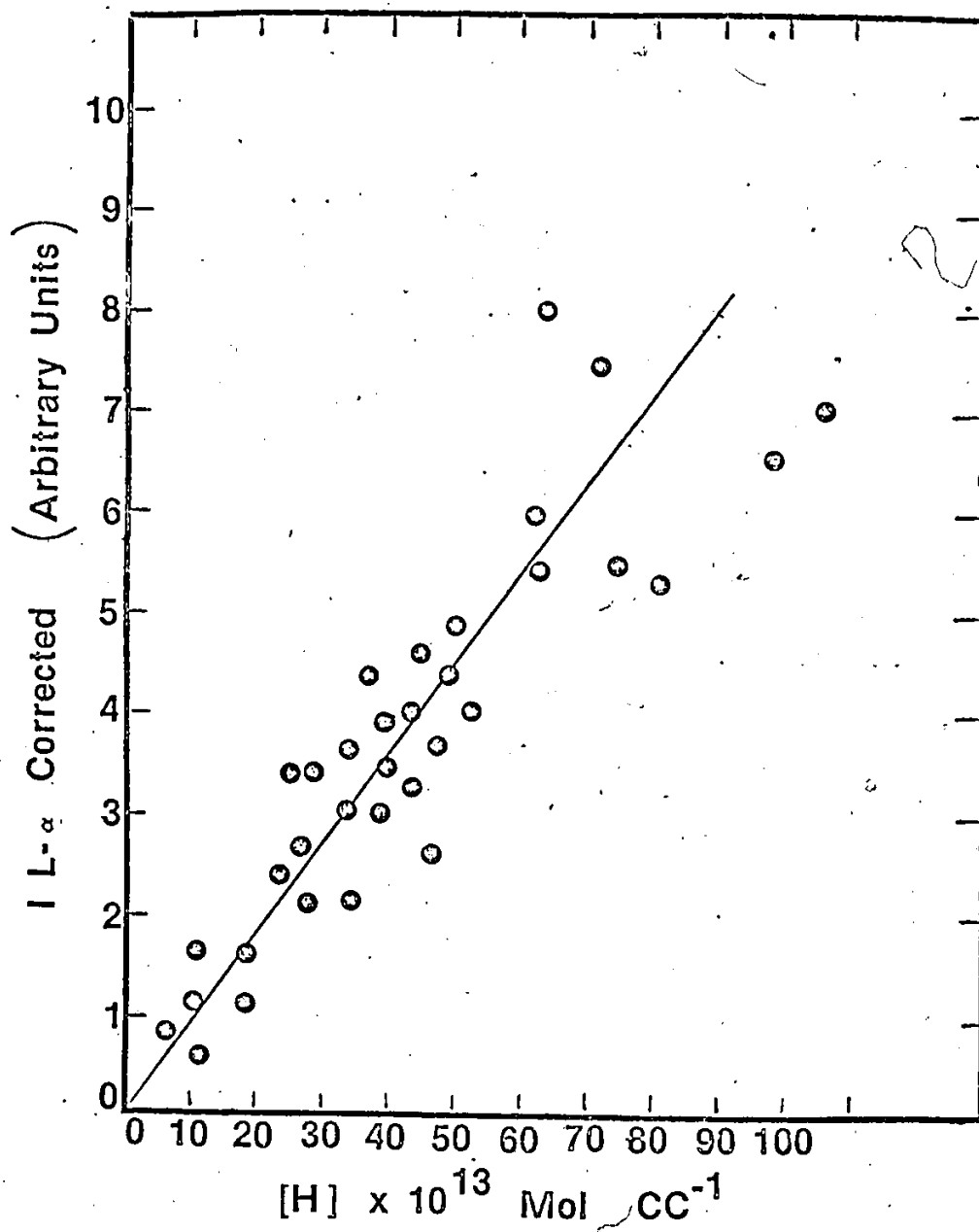


Fig. 12.
Calibration Curve of Absolute [H]

f) HIGH RESOLUTION SPECTRA

A typical resolved resonance fluorescence rotational spectrum is shown in Fig. 10 for the (3,4) band. Generally in all spectra observed, rotational separation was poor and line broadening effects added to the poor resolution. In many cases the R(0) ($J'=1$), R(1) ($J'=2$) and the P(1) ($J=0$) and R(2) ($J=3$) could not be adequately separated (see Fig. 10). A further complication encountered was overlapping orders. Measurements were mainly made in the fourth order since this afforded the best resolution, intensity and reproducibility of the Lyman bands. A commonly occurring problem was the overlapping of the electronic transition from upper vibrational bands in the third order (see Fig. 9). This was particularly a problem for the (3,1) band where interference is observed from the third order (3,8) band in the region 111.2 to 112.4 nm, similarly the R(0) and R(1) branches of the (3,3) band overlaps the Lyman-line and the third order (3,11) interferes from 122.5 to 122.8 nm.

Table 5 shows the observed and relative intensities of the rotational lines for the (3,4) band for a range of pressures studied in a series of experiments.

Despite the difficulties of unresolved peaks and broadened lines, a general trend does emerge. The normalized high resolution line intensities as shown in Fig. 10 and listed in Table 5 indicate that the bulk

Table 5. Observed and relative intensities of Argon sensitized fluorescence of Hydrogen for $v'=3, v''=4$ of the Lyman band emission. Values listed correspond to values for the (3,4) band under high resolution for a range of pressures.

Notes from Table:

- (a) Observed arbitrary units, I
- (b) Normalized to most intense line, I_N
- (c) Observed in 4th order
- (d) Unresolved J levels
- (e) 3rd order interference

TABLE 5
Observed and relative intensities

(nm) (c)	J'	Branch	I ^(a)	I _N ^(b)
126.85 (d)	1	R(0)	46.0	89
126.89 (d)	2	R(1)	46.0	89
127.04 (e)	3	R(2)	51.2	99
127.31 (e)	1	P(2)	51.6	100
127.28 (e)	4,0	R(3), P(1)	51.6	100
127.66	2	P(3)	37.6	73
128.11	3	P(4)	14.0	27
128.64	4	P(5)	3.9	8

Partial pressure of Hydrogen = 0.549 kPa

Total pressure = 3.53 kPa

TABLE 5
Observed and relative intensities

(nm) (c)	J'	Branch	I ^(a)	I _N ^(b)
126.85 (d)	1	R(0)	3.1	67
126.89 (d)	2	R(1)	3.1	67
127.04 (e)	3	R(2)	4.6	100
127.31 (e)	1	P(2)	4.5	98
127.28 (e)	4,0	R(3), P(1)	4.5	98
127.66	2	P(3)	2.6	57
128.11	3	P(4)	2.3	50
128.64	4	P(5)	1.0	22

Partial pressure of Hydrogen = 3.48×10^{-3} kPa

Total pressure = 5.00 kPa

TABLE 5
Observed and relative intensities

(nm) (c)	J'	Branch	I (a)	I _N ^(b)
126.85 (d)	1	R(0)	14.7	60
126.89 (d)	2	R(1)	14.7	60
127.04 (e)	3	R(2)	24.3	100
127.31 (e)	L 1	P(2)	16.6	68
127.28 (e)	4,0	R(3), P(1)	16.6	68
127.66	2	P(3)	16.7	69
128.11	3	P(4)	5.1	21
128.64	4	P(5)	2.4	10

Partial pressure of Hydrogen = 2.98×10^{-2} kPa

Total pressure = 4.53 kPa

TABLE 5
Observed and relative intensities

(nm) (c)	J'	Branch	I (a)	I _N (b)
126.85 (d)	1	R(0)	8.1	49
126.89 (d)	2	R(1)	8.1	49
127.04 (e)	3	R(2)	11.0	66
127.31 (e)	1	P(2)	16.7	100
127.28 (e)	4,0	R(3), P(1)	16.7	100
127.66	2	P(3)	8.6	51
128.11	3	P(4)	3.8	23
128.64	4	P(5)	1.0	6

Partial pressure of Hydrogen = 2.57×10^{-2} kPa

Total pressure = 2.27 kPa

TABLE 5
Observed and relative intensities

(nm) (c)	J'	Branch	I (a)	I _N ^(b)
126.85 (d)	1	R(0)	2.5	43
126.89 (d)	2	R(1)	2.5	43
127.04 (e)	3	R(2)	5.8	100
127.31 (e)	1	P(2)	2.2	38
127.28 (e)	4,0	R(3), P(1)	2.2	38
127.66	2	P(3)	4.1	71
128.11	3	P(4)	1.3	22
128.64	4	P(5)	1.2	21

Partial pressure of Hydrogen = 0.160 kPa

Total pressure = 14.1 kPa

TABLE 5
Observed and relative intensities

(nm) (c)	J'	Branch	I (a)	I _N ^(b)
126.85 (d)	1	R(0)	14.8	77
126.89 (d)	2	R(1)	14.8	77
127.04 (e)	3	R(2)	19.1	100
127.31 (e)	1	P(2)	16.8	88
127.28 (e)	4,0	R(3), P(1)	16.8	88
127.66	2	P(3)	14.7	77
128.11	3	P(4)	6.6	35
128.64	4	P(5)	1.0	5

Partial pressure of Hydrogen = 0.505 kPa

Total pressure = 4.00 kPa

TABLE 5
Observed and relative intensities

(nm) (c)	J'	Branch	I (a)	I _N ^(b)
126.85 (d)	1	R(0)	15.2	57
126.89 (d)	2	R(1)	15.2	57
127.04 (e)	3	R(2)	5.8	22
127.31 (e)	1	P(2)	26.7	100
127.28 (e)	4,0	R(3),P(1)	26.7	100
127.66	2	P(3)	3.2	12
128.11	3	P(4)	1.0	4
128.64	4	P(5)	1.0	4

Partial pressure of Hydrogen = 4.47 kPa

Total pressure = 4.47 kPa

TABLE 5
Observed and relative intensities

(nm) (c)	J'	Branch	I (a)	I (b)
126.85 (d)	1	R(0)	0	0
126.89 (d)	2	R(1)	0	0
127.04 (e)	3	R(2)	0	0
127.31 (e)	1	P(2)	0	0
127.28 (e)	4,0	R(3), P(1)	0	0
127.66	2	P(3)	0	0
128.11	3	P(4)	0	0
128.64	4	P(5)	0	0

Partial pressure of Hydrogen = 0.0 kPa

Total pressure = 0.0 kPa

of the rotational population is distributed nearly evenly for $J' < 4$ and that levels $J' > 4$ are unpopulated. This effect correlates well with the energy defect diagrams (Fig. 14 and Fig. 15), where the largest intensity comes from the smallest energy defect.

At higher pressures lower rotational levels are more populated, (ie the population decreases with increasing J' levels). At total pressures of over 1.3 kPa, the rotational levels $J'=0,1,2$ are populated to a larger extent than $J'=3,4,5$ and there is no indication of any population of $J' \geq 5$ observed.

For the case of "pure" hydrogen, similar fluorescence spectra appear, however the intensity of the rotational levels is shifted and considerably lower than for the H_2/Ar mixtures as shown in the much lower intensity values for R(2) and P(4). In H_2/Ar mixtures, these levels are considerably more intense. The population seems to be predominantly in $J'=0,1$, for this case (pure H_2 , $[Ar] \ll 10$ ppm).

Other workers (27), (28), (61) using discharges have observed additional enhanced progressions along with the Lyman bands. These were: the $v''(v'=0)$ progression of $C^1\Pi_u \rightarrow X^1\Sigma_g^+$ (Werner bands) system with individual bands containing two enhanced lines, R(0) and P(2) and also the $v''(v'=5)$ progression of the $B^1\Sigma_u^+ \rightarrow X^1\Sigma_g^+$ system. These other bands are somewhat weaker than the Lyman bands (27) and were not observed in our system. The Werner bands are excited by the 104.8 nm Ar^* and we

FIG. 13. Decay plot of Lyman- α fluorescence during an experiment. Data is obtained from Table 4.

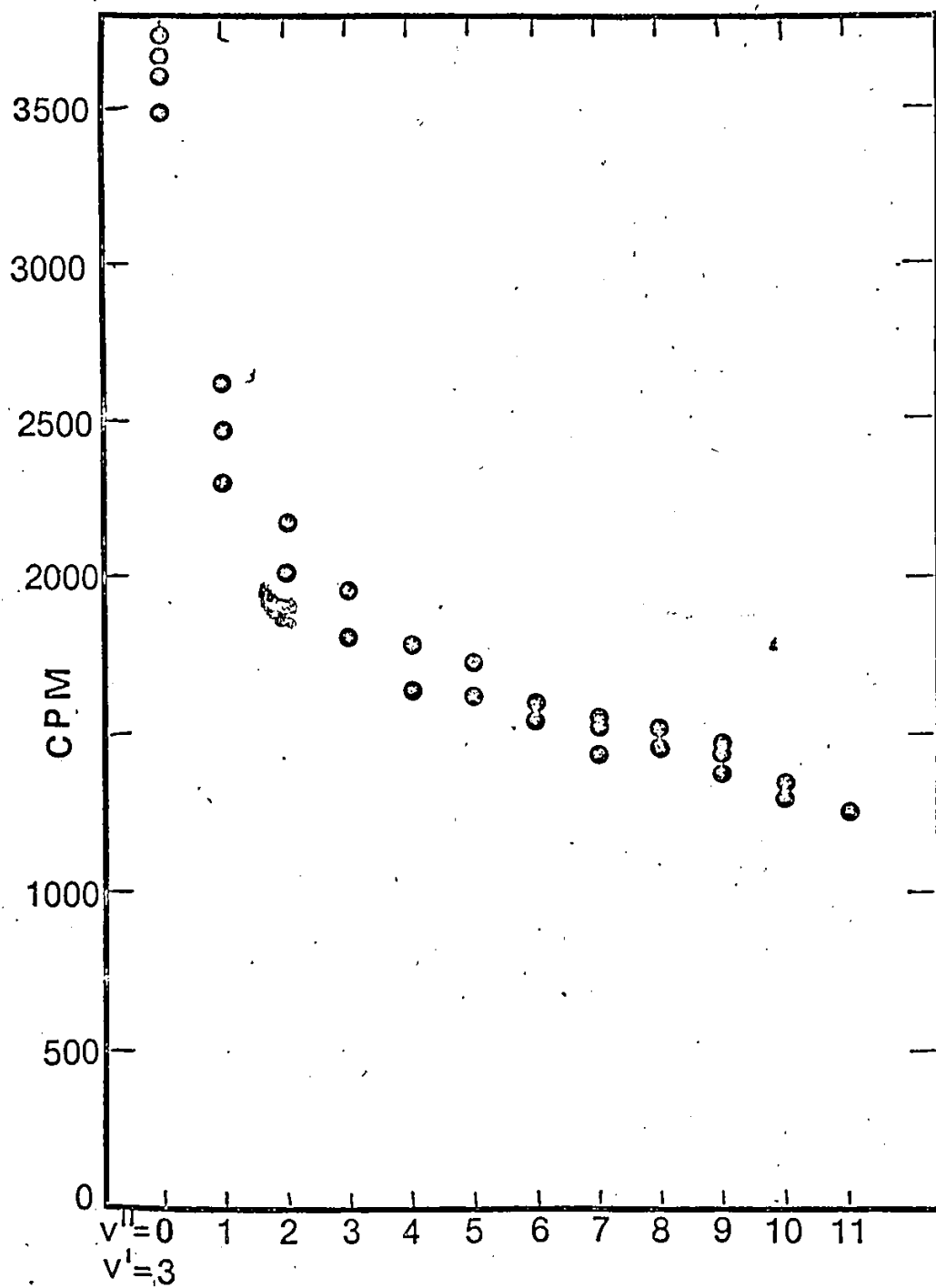


Fig. 13.
Decay Plot of Lyman - α Fluorescence

FIG. 14. Resonance defects (a), Δv , of the B state of Hydrogen and the 106.7 nm resonant state of Argon. $B_v^{J'}$ and $X_v^{J''}$ represent the excited and ground state of H_2 respectively. v, J are the respective vibrational and rotational quantum numbers. Solid lines indicate optically allowed transitions, broken lines represent optically forbidden transitions.

(a) From reference 25.

Ar* [106.7 nm] Resonance State ($\text{Ar}^* [^3\text{P}_1]$)

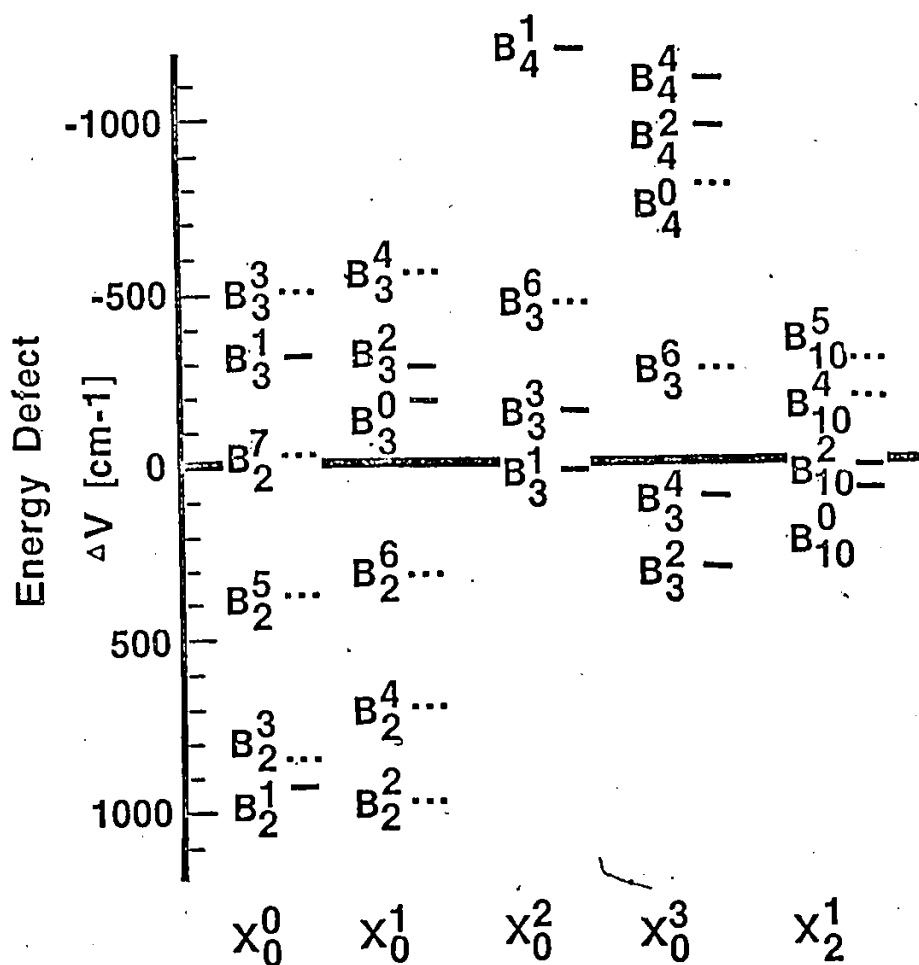
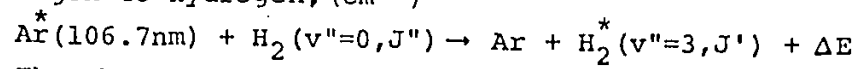


Fig. 14.

Resonance Defects ΔV of B State Hydrogen

FIG. 15. Energy defects (from Ref.33) for
electronic energy transfer from
Argon to Hydrogen, (cm^{-1})



The observed transitions are
indicated by bold type.

J''	J'					
	0	1	2	3	4	5
0		-334		-501		-798
1	-181		-282		-515	
2		21		-147		-443
3	406		305		72	
4		835		669		371
5	1441		1339		1106	
6		2081		1914		1617

Fig. 15.
Energy Defects
(From Ref. 33)

would not expect to observe these transitions.

The observed selective enhancements of the H_2^* bands can be explained by Kallman and London's theory of resonance excitation (52). The transitions should follow optical selection rules except that for rotational angular momentum which will not be as rigid as for the case of optical transitions (28). The resonance defects Δv of rotational levels in the B state determine the efficiency of excitation and are located within 600 cm^{-1} of the 3P_1 state of Ar shown in Fig. 14.

These resonance defects (Fig. 14) are similar to those shown in Kallman and London's article (51) but corrected for rotational levels (62) and later revised by Takezawa et al. (28). Here B_3^1 , B_3^4 , B_{10}^2 have small values in this defect; and the transitions with their respective lower states, also shown in Fig. 14 and 15 are all optically allowed. Therefore, according to the given theory, it is expected that lines originating on these upper levels will be enhanced i.e. selectively excited by collisions of Ar* atoms in the 3P_1 state with the ground state of H_2 ($v=0, J''$). Experimentally, this was observed for the $v'=3$ cases, however for $v'=10$, no emission was observed. Also, as indicated in Fig. 14 the magnitude of this resonance defect for the B_3^1 level (which shows enhancement) is nearly equivalent to that of the B_{10}^2 , for which no enhanced lines were observed in these experiments. One of the reasons for this is that the initial level for the process leading to B_{10}^2 must

be x_2^1 while for the other (observed) cases, the ground state is x_0^1 , x_0^2 , x_0^3 and the population of H_2 molecules in level $v'=2$, $J'=1$ is virtually zero at room temperature.

This is demonstrated by the emission observed for the (3,4) band. For the ground state, x_0^3 , $\Delta v = 72 \text{ cm}^{-1}$, a similar energy defect is given for the (10,0) band with the x_1^2 ground state. The (10,0) band occurs at 141.3 nm (within our sensitivity range although low) but no emission was observed.

It was found that the most intense emission was observed for the transitions with the smallest energy defects. In the $v''(v'=3)$ transition, fluorescence was observed to decrease as the energy defect for electronic energy transfer increased. The energy defects are shown in Fig. 14 and Fig. 15.

The line widths in the spectra observed are important sources of information about transitions in collisions. Pure rotational lines depend mostly on the total rate of inelastic collisions. A few percent of the pure rotational broadening arises from re-orientation of the angular momentum, without changes in the magnitude of the rotational angular momentum, through amplitude modulation of the line (63). Widths of the rotation-vibration spectral lines are often broadened due to vibrational phase shifts in collisions.

The line widths of rotational spectra are dependent on other factors such as the natural lifetime of the states, Doppler broadening and collision broadening.

Collision broadening is the dominant factor for rotational lines at pressures greater than one micron (64).

The sensitivity of the detection system also contributes to the weakness of the intensity observed (see Fig. 6). Similar observations may also be noted for other weak bands.

Because of the deterioration of reflectance of the optics of the monochromator (deterioration of MgF_2 coating on mirrors and grating resulting from leaks that occurred in the system) the Ar resonance lines could not be observed in the lamp discharge. The resonance defects of the levels which produced enhanced lines are expected to be within the widths of the Ar resonance lines, the upper states of which correspond to Ar^* (106.7 and 104.8 nm). Enhancement is produced by collisions of Ar^* with H_2 at the indicated lower levels shown in Fig. 14, (33), (40), (28), (27). The relative importance of these two levels is difficult to determine, although owing to the behaviour of the Li F windows and subsequent colour centre formation, it is probable that the $\text{Ar}(^3\text{P}_1)$ resulting from absorption of the 106.6 Ar resonance line is the dominant species.

Loss of transmission through the fluorescence cell was a constant problem. Fig. 13, referred to previously, shows a typical $\text{L}-\alpha$ decay plot representing these transmission losses.

Resonance emission quenching experiments are under-

taken in order to determine whether quenching is present and to the extent of quenching thus giving clues to the mechanistic behaviour of the system and a numerical value for the quenching.

At higher pressures, there is evidence of quenching, however more data is required to determine a precise estimate of the effect of quenching.

Mitchell and Zemansky (50) emphasize that a quenching curve, by itself, without further details as to line breadths, geometry of the apparatus, side reactions ($2H + wall$), etc. can give no information of an absolute nature whatsoever, and indeed in some cases is not convincing evidence that quenching takes place at all.

CONCLUSIONS

In this experiment resonance excitation of H_2 molecules by optically excited Argon atoms created H_2^* in the excited electronic-vibration-rotation state of $B \sum_u^+$, $v'=3$, $J'=0 \rightarrow 4$ where Ar^* is optically excited at 106.7 nm and the hydrogen molecules are initially distributed among low J levels. Spontaneous emission occurs which returns the molecules directly to the ground electronic state from the level pumped. The spectrum that results is very simple and can be easily identified. At higher pressures, some evidence of quenching is observed but more extensive experimentation would be required with additional quenching gases over a very wide.

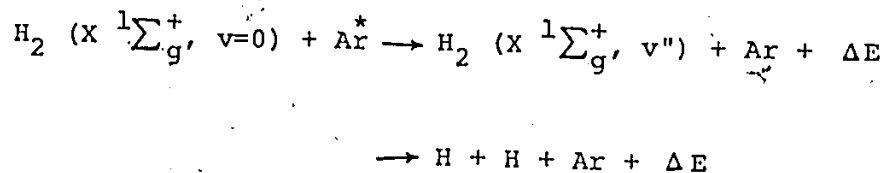
range of pressures in order to thoroughly elucidate this behaviour and obtain relative quenching efficiencies of the species used.

Energy transfer experiments are very important and critical to our understanding of the interaction of energy with matter. Electronic energy may be transferred from an optically excited rare gas atom to a molecular species by collision and the effects monitored by observation of a fluorescence spectrum over a wide range of pressures.

Fink, Wallach and Moore (33) studied argon sensitized fluorescence of H_2 and were able to obtain a range of cross sections which were normalized to the largest calculated ones of 45.5 \AA^2 for $HD^*(v'=3, J'=2)$ excited by Ar^* (106.7 nm) and of 137 \AA^2 for $HD^*(v'=5, J'=2)$ for Ar^* (104.8 nm) level. The absolute magnitude of these cross-sections was estimated by using long range dipolar calculations utilizing first order time dependent perturbation theory and assuming a straight line constant velocity trajectory. They found that generally only one vibrational level of the hydrogen molecule is excited by each argon state which sharply contrasts many previous sensitized excitation experiments where excitation was observed in most of the energetically accessible energy levels (27), (29), (48), (61).

This report confirms the resonant excitation process that is observed for $v'=3, v''$ Lyman bands and indicates the relative population distribution of the rotational

levels of ground state H_2 . There is also evidence that the mechanism concerned with the energy transfer does indeed involve H atoms with an efficiency of approximately 5% as important as production of H_2^* . Fink et al. (33) neglected the processes



which can compete with energy transfer.

In order to fully understand and substantiate the kinetics involved, extensive further experimentation would be necessary. In particular, a thorough understanding of the part that hydrogen atoms play in this system, requires a well defined reactor wall surface.

Furthermore, in order to prevent $L-\alpha$ decays in the reactor, an all glass system would be required, adequately coated to prevent heterogeneous recombination of H atoms. Ideally, a windowless system would optimize measurement of Lyman- α and exciting radiation and eliminate the undesirable effects caused by colour centre formation in lithium fluoride windows. This would also increase sensitivity and open a wide wavelength range for which to study sensitized fluorescence. Unfortunately the difficulties encountered in windowless systems utilizing differential pumping and pressure requirements overshadow this proposed technique. Realistically a new

design incorporating easily replaceable LiF windows could be devised.

In order to provide optimum conditions for energy transfer studies, two different experimental set-ups would be required. One would resolve the sensitized fluorescence light spectroscopically and another would provide the necessary versatility to select a single emission line from the lamp to be used for excitation.

In observing the fluorescence intensity, the cell must be long enough to permit absorption studies and should also have the same aperture ratio of the monochromator. The latter design modification prevents the absorption of exciting radiation by gas molecules unable to emit in the solid angle subtended by the monochromator. (40).

In order to obtain the necessary spectral purity, Ultra High Purity Argon gas is required for the lamp which should be operated at pressures no greater than 7×10^{-1} Pa, (several orders of magnitude lower than in the present experiments). The low lamp pressure would create a sharp exciting line necessary for critical measurements.

The present McPherson 0.3 m monochromator would be excellent for resolving the exciting lines present in the Argon discharge to be used for excitation, however for sensitive vibrational and rotational transfer processes a 1 m McPherson Model 225 scanning vacuum - uv monochromator would be desirable whereas a 3 m

normal-incidence vacuum spectrograph equipped with a 1200 line/mm grating as employed by Tanaka et al. (38) would be ideal. Under these conditions further experimentation would be desirable.

APPENDIX AMICROWAVE-EXCITED ARGON EMISSION CONTINUUM

The production of an intense continuum source in the vacuum ultraviolet from 105.0 -140.0 nm offers an excellent technique for the possible studies of species that absorb in this region. Interest in vacuum uv absorption spectroscopy has stimulated research for the development of emission continua of the noble gases. Of particular importance in the measurement of complicated molecular absorption and ionization cross-section is the development of intense, stable continuum background light sources for photoelectric scanning with vacuum monochromators. Under the proper conditions, all of the rare gases will emit continuous spectra with only a few emission lines which may be used as wavelength standards. Both condensed and microwave discharges can be used for excitation of such continua.

Research on condensed discharges in rare gases has been carried out by Tanaka et al. (65) and by Newburgh (66). Older reviews concerning studies carried out on vacuum ultraviolet continuum sources have been carried out by Huffman et al. (67). An excellent work on rare gas continuum sources for the vacuum ultraviolet using Xenon, Krypton and Argon was reviewed by Wilkinson and Byram (68) who elaborated upon the theory and production of microwave excited continua.

In this work, the continuum lamp was designed somewhat similarly to that of Wilkinson et al. (68). Slight

modifications were made in order to allow for the low melting temperature (725°C) of the Ba getter and high uv discharge power used.

ARGON CONTINUUM LAMP

The argon continuum lamp Fig. 16 was designed with the incorporation of a quartz side arm and a quartz discharge zone. The lamp was rinsed in a concentrated HF solution followed by soaking for approximately 2 hours in a 10% HF solution. Another rinsing with concentrated HF was followed by repeated rinsings with distilled water for at least 15 minutes. The lamp was placed in a drying oven for approximately 2 hours at 120°C . After the lamp was taken from the drying oven and allowed to cool, Lepage's Epoxy glue was used to fix a 1 mm thick LiF (Harshaw Mfg.) window to the lamp. Approximately 4 granules of getter (Barium 99.5%) obtained from Ventron-Alpha Products, Beverly, Mass., USA were placed in the side arm. The lamp was positioned into the apparatus and connected to the argon line by glass blowing using a positive pressure of Ar. Heating tape was wrapped around the lamp and allowed to heat up to approximately 400°C for six hours while being pumped on. A small flow of argon was allowed to pass through the lamp while heating and pumping. The lamp was then left under vacuum for a day and the pressure monitored in order to be sure that no leaks were present. Heating

FIG. 16. Schematic diagram of Argon continuum lamp used for production of Argon continuum.

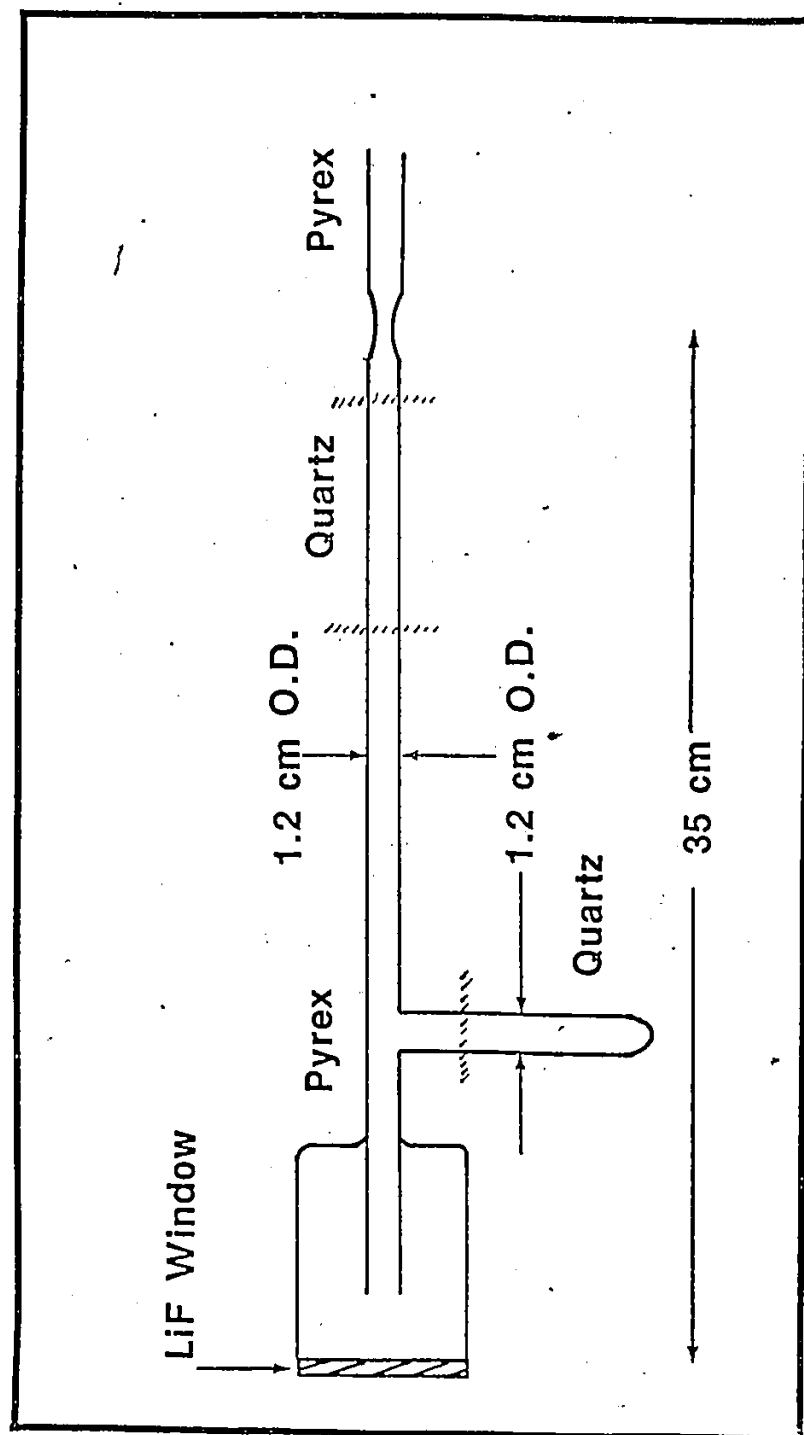


Fig. 16.
Schematic Diagram of Argon Continuum Lamp

(450°C) was again applied and ultrapure argon (impurity level < 5 ppm) was allowed to flow through the lamp for approximately six hours. The heating element was turned off and the lamp was allowed to cool slowly. Similarly a molecular sieve arrangement which was used to further purify the Ar was degassed at ~350°C and allowed to cool slowly. The Ba getter in the side arm was then carefully fired in the side arm until all the Ba was vapourized and deposited along the walls of the side arm lamp. Ultrapure Argon (Gas Dynamics) was then added to the lamp through the molecular sieve trap at -178°C. The lamp was then isolated when the pressure in the Ar flow line stabilized to 2.7×10^{-4} Pa and the lamp was then carefully sealed off. Spectra of the Ar continuum were taken while an additional discharge was activated at the side arm of the lamp. The discharging at the side arm was continued until a maximum value of the continuum intensity was achieved.

In previous lamp designs, the main problem encountered was cracking of the side arm. This was due to the differences in the coefficients of expansion of pyrex and Ba as a result of fusion of the getter into the walls of the pyrex side arm after heating. (The melting point of Barium is 725°C (7) and the softening point of borosilicate glass (Kimax and Pyrex) is approximately 820°C (69). This caused the Ba to fuse to the glass and upon cooling the side arm usually cracked due to thermal stress.

Fig. 17 shows the intensity distribution in the continuous emission spectrum of Argon excited by microwave discharge (17 W). Careful measurements of the emission intensity of the Argon continuum as a function of pressure (68) revealed that the intensity of the long wavelength maximum increased approximately logarithmically with pressure in the range from 1.33×10^4 Pa to 5.67×10^4 Pa. However, the contrary was true in the short wavelength region where the intensity decreased with pressure rather rapidly up to 5.33×10^4 Pa before leveling off. The optimum pressure was found to be approximately 2.67×10^4 Pa.

Another factor affecting the intensity of the continuum source is the presence of impurities. Ordinary atmospheric and chemically active gases (nitrogen, carbon dioxide, hydrogen, oxygen, carbon monoxide, and water vapour) all borrow intensity from the continuum and manifest themselves as atomic lines over the wavelength region of interest. These gases are absorbed by the getter as physisorption or chemisorption (70) which, in most cases, can be considered irreversible unless the condensed getter surface is reheated to a temperature much higher than would normally be encountered or is bombarded by electrons.

The pressure in the lamp at the time of flashing the getter will determine the appearance and condition of the condensed deposit. Very slow heating of the getter results in absorption of most of the residual

FIG. 17. Argon continuum with impurity resonance lines; Microwave discharge: 50W, Slit width: 21 microns.

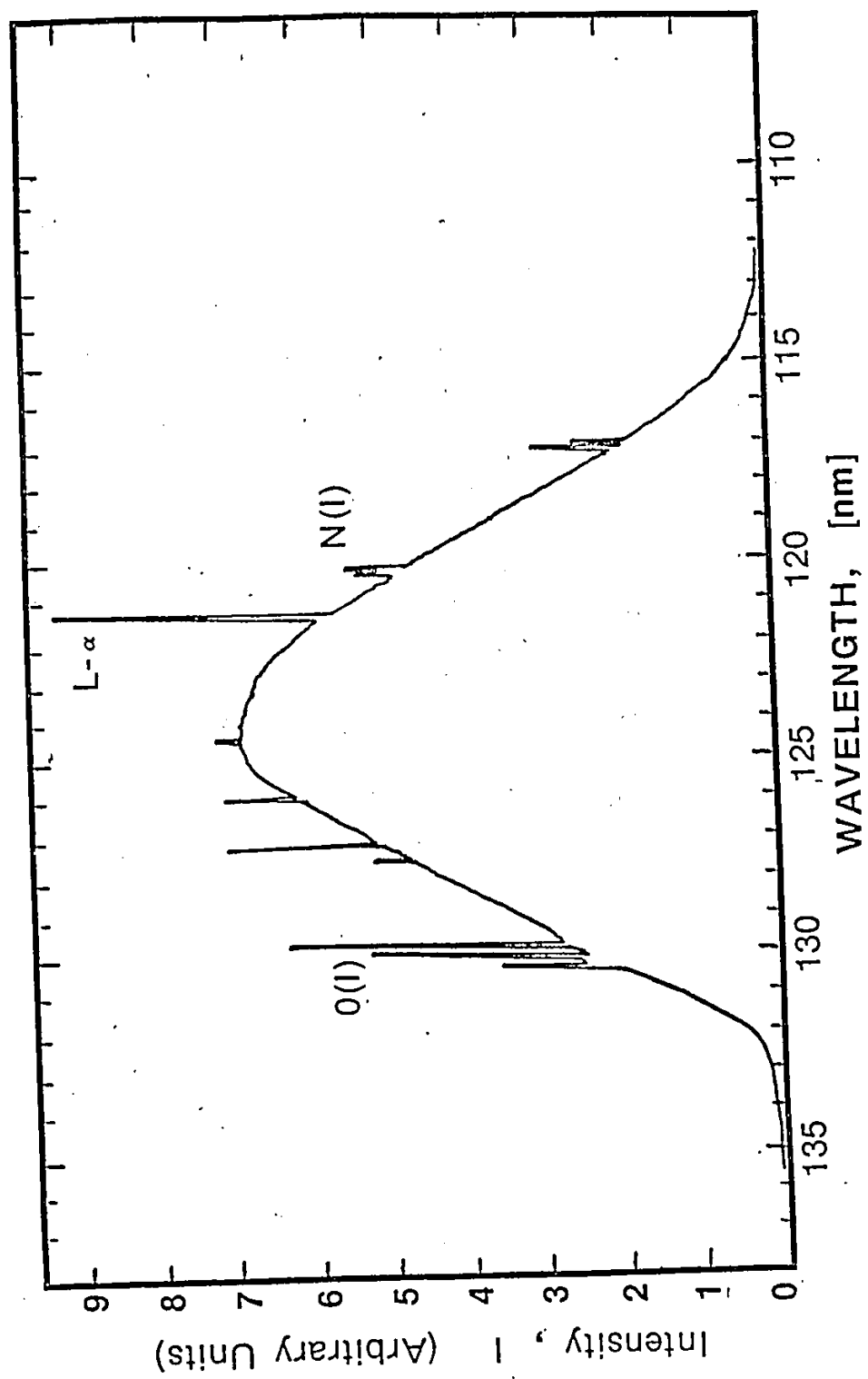


Fig. 17.
Argon Continuum with Impurity Resonance Lines

impurity gas in the tube before much condensation which, under these conditions presents a bright mirror appearance. However, if the temperature of the getter is raised very rapidly, condensation occurs before the getter action can operate completely, and this results in a discoloured mirror appearance. In all cases using Ar in the lamp, flashing of the getter produces a black deposit in the region exposed to heating which is not contaminated but porous and light absorbing.

Fig. 18 illustrates the effects of N impurity and the change in intensity upon elimination of nitrogen by the Ba getter. It was found that continuous discharging of the side arm containing getter helped eliminate atomic nitrogen peaks and increased the maximum intensity of the Argon continuum by about 75%.

ABSORPTION MEASUREMENTS

The lowest lying stable excited state of Hydrogen is $B^1\Sigma_u^+$. Strong absorption occurs from 112.5 nm and continues to longer wavelengths. (68). The rotational structure may nearly be completely resolved due to the small moment of inertia (large B_v), even with a 1 m. monochromator (68).

Attempts were made at observing the absorption spectrum $H_2^*(B \leftarrow X)$ in the pressure range of 133 to 6.65×10^4 Pa total pressure of various H_2 /Ar mixtures and in pure H_2 . The sensitized resonance fluorescence

FIG. 18. Effect of microwave discharge at the sidearm containing Ba getter on the intensity distribution of the Argon continuum (—————).

(a) Continuum showing nitrogen impurity lines.

(b) Effect observed after continuous discharge of Ba getter for 2 hours (- - - - -).

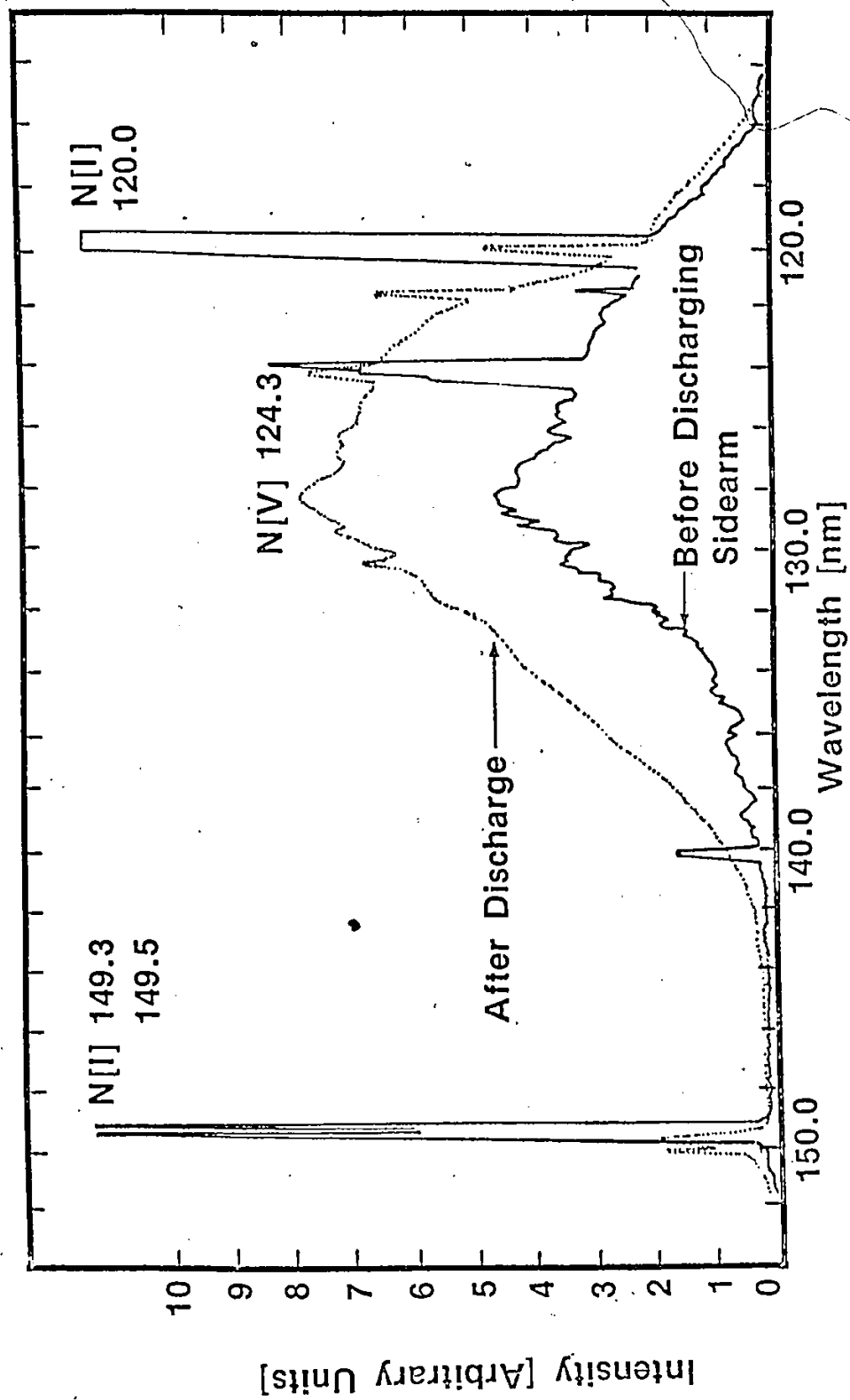


Fig. 18.
Effect of Microwave Discharge

technique was used to excite hydrogen into the $B^1\Sigma_u^+$ state and continuous scans (0.1 nm min^{-1} to 2 nm min^{-1}) were taken over the pressure ranges studied. No absorption of H_2^* was observed under these conditions.

APPENDIX B

DETECTING SYSTEM CALIBRATION

Many techniques have been developed for intensity measurements and calibration of optical systems for different regions of the electromagnetic spectrum. To determine absolute intensities, a detector with a known absolute response must be used. The detector must be an "absolute detector" or one which can be calibrated against a standard source of known intensity.

Measurements in the visible and infrared regions are usually straightforward and require only a comparison of the radiation from the unknown source to that emitted from a standard lamp. These techniques are useful to about a lower limit of 300 nm. At this limit and in lower regions, great care is necessary due to low intensity outputs of standard lamps such as the quartz iodine standard lamp which is commonly used in the ultraviolet. In the region from 100 to 300 nm, the calibration of an optical system was, until recently, extremely difficult, mainly due to lack of primary standards. Excellent reviews have been published on absolute and relative intensity measurements in the vacuum ultraviolet by Samson (71) and Shreider (72) and reference should be made to these sources for specific details.

A thermocouple may be used as a primary standard since its response in microvolts is independent of wave-

length over a wide range (soft Xrays to I.R.), but it must be calibrated against a standard source. Other types of absolute detectors include, rare gas photoionization detectors, ion chambers of various designs, photon counters and a Golay Cell (essentially a gas thermometer consisting of a mirror and flexible membrane).

Line ratios can be used to determine absolute intensities if the transition probabilities of two lines with a common upper level are known, as well as the intensity of one of the lines. The intensity of the unknown line can then be determined. This technique requires an optically thin source, accurately known transition probabilities, known spectral emission from a standard lamp, and known population distribution among any unresolved fine structure sub levels of the upper level.

The most commonly used technique in intensity calibrations has been the atomic branching ratio-technique. This method has the disadvantage of giving only a few scattered calibration points over a wide wavelength range and also requires two optical systems: one to calibrate the long wavelength atomic line intensity (usually He 501.5 nm) and the other for use in the vacuum ultraviolet (usually 58.4 nm). In this method, two monochromators are used, with the exit slit of the first becoming the entrance slit of the second. The output of the first monochromator is measured by some non-selective energy-sensitive device such as a thermocouple or bolometer and this becomes a calibrated light source

for the second monochromator.

MOLECULAR BRANCHING RATIO METHOD

A much simplified technique has been suggested by J. W. McConkey (56). He proposed that the atomic-branching ratio technique be extended by using molecular rather than atomic emissions originating at the same upper state and by making use of the corresponding molecular transition probabilities or Franck-Condon factors. This provides a relative intensity calibration over the wavelength range that molecular emission is observed. He obtained reasonably good agreement for the relative quantum efficiency of the detecting equipment (300 - 450 nm) using the intensity of second positive bands of Nitrogen $N_2(C^3\Pi_u - B^3\Pi_g)$ compared to the spectral response obtained using a NBS standard quartz-iodine lamp. This method was also carried out independently by Aarts and deHeer (73) using the CO(A $^1\Pi - X^1\Sigma^+$) fourth positive group from 158 to 260 nm. They suggested that by using a mercury standard, an absolute scale could be introduced achieving an accuracy of approximately 10%.

Recently Mumma and Zipf (74) excited the Lyman-Berge-Hopfield system of $N_2(a^1\Pi_g - X^1\Sigma_g^+)$ and the CO fourth positive system (A $^1\Pi - X^1\Sigma^+$) by low energy electron impact (100 eV). The emission bands of these molecular systems are spread uniformly over the wavelength region

from 115 - 250 nm, and the absolute transition probabilities (75) for both these systems are known, thus making relative measurements of the intensity of these bands a convenient technique for calibrating vacuum ultraviolet detecting apparatus.

These relative intensity measurements can be placed on an absolute basis by directly comparing the band intensities to the intensity of the hydrogen Lyman- α line (121.56 nm) and the O(I) resonance triplet (130.2, 130.4, 130.6 nm) produced by dissociative excitation (76), (77) of hydrogen and oxygen, and also to a standard lamp (74) at wavelengths greater than 150 nm. Under these conditions Mumma and Zipf claim that the sensitivity of a monochromator could be determined over this wavelength range with an absolute accuracy of $\pm 10\%$.

CALIBRATION OF THE DETECTION SYSTEM USED IN THIS WORK

The Branching Ratio Method was well suited for calibration of the detection system used in this work. Fluorescence of the Lyman system $v'=3, v''$ ($B^1\Sigma_u^+ \rightarrow X^1\Sigma_g^+$) provided a well defined band progression in the wavelength range from approximately 105.0 nm to 165.0 nm and the corresponding Einstein transition probabilities have been calculated by Allison and Dalgarno (55), (56).

The emitted intensity (56) of an emission band is given by:

$$[33] \quad I_{v',v''} = CN_{v'} E_{v',v''}^3 \bar{R}_e^2 q_{v',v''} \quad (\text{photons/sec})$$

where C is a constant, $N_{v'}$ is the population of the upper vibrational level v' , v'' is the lower vibrational level, $E_{v',v''}$ is the energy difference between v' and v'' , \bar{R}_e is the average value of the electronic transition moment, and $q_{v',v''}$ is the Franck-Condon Factor. \bar{R}_e^2 may be regarded as effectively constant even though it varies slowly within a given band system.

The transition probability (78), $A_{v',v''}$ is given by:

$$[34] \quad A_{v',v''} = \left(\frac{64 \pi^4}{3h} \right) E_{v',v''}^3 \bar{R}_e^2 q_{v',v''} \quad (s^{-1})$$

By combining equation [33] and [34], the volume emission rate may be given as

$$[35] \quad I_{v',v''} \propto N_{v'} A_{v',v''} \quad (\text{photons cm}^{-3} \text{ s}^{-1})$$

The intensity ratio of two lines or bands originating from the same upper level relates to the ratio of their corresponding Einstein transition probabilities

$$[36] \quad \frac{I_{(v',v'')_1}}{I_{(v',v'')_2}} = \frac{(A_{v',v''})_1}{(A_{v',v''})_2}$$

The lifetime of the vibrational level, v' is $\tau_{v'}$, where $\tau_{v'} = (A_{v'})^{-1}$ and

$$[37] \quad \frac{1}{\tau_{v'}} = A_{v'} = \sum_{v''} A_{v',v''}$$

Individual $A_{v',v''}$ values are obtained from $A_{v'}$, by use of measured vibrational band emission intensities, $I_{v',v''}$ (quanta per second) as in [36] .

If the emission is incident on a detecting optical system (windows + monochromator + detector) having a spectral sensitivity of $k(\lambda)$, then the measured detector response (counts/sec) for a band (v',v'') at wavelength λ is given by

$$[38] \quad S(\lambda) = Gk(\lambda_{v',v''}) I_{v',v''}$$

The value G corresponds to a geometrical function involving the solid angle of the optical system, lamp and window characteristics, monochromator slit settings, etc. In determination of relative spectral response, G is kept constant for observations of a given band system and its effect is thus cancelled.

Comparison of two different bands having wavelengths of λ_1 , and λ_2 gives :

$$[39] \quad \frac{S(\lambda_1)}{S(\lambda_2)} = \frac{k(\lambda_{v',v''})_1 (I_{v',v''})_1}{k(\lambda_{v',v''})_2 (I_{v',v''})_2}$$

The relative intensities of emission lines $\frac{S(\lambda_1)}{S(\lambda_2)}$

of a particular band is used to calculate the relative sensitivity $\frac{k(\lambda_{v'v''})_1}{k(\lambda_{v'v''})_2}$ of the particular band system.

The sensitivity of the strongest line $S(\lambda_2)$ is normalized to 1.

Rearranging equation [39] and substitution into equation [36], the following expression is obtained:

$$[40] \quad \frac{k(\lambda_{v'v''})_1}{k(\lambda_{v'v''})_2} = \left\{ \frac{S(\lambda_{v'v''})_1}{S(\lambda_{v'v''})_2} \right\} \times \left\{ \frac{A(v'v'')_2}{A(v'v'')_1} \right\}$$

Thus the relative spectral response, $\frac{k(\lambda_{v'v''})_1}{k(\lambda_{v'v''})_2}$ of the optical system can be determined for a given v'' progression, independent of the way in which the various v' are populated.

Recently single rotational levels in the H_2^* B-state ($v'=3, J'=1$) have been excited by Becker et al. (58) by using monochromatic excitation of H_2 by the 106.6 nm Argon resonance line. The emitted (B-X) radiation consisted of one P-branch line and one R-branch line for each transition ($3, v''$). Using "ab initio" calculations of the transition probabilities (55) and line intensities, Becker et al. showed that a calibration curve established using the Lyman lines was in good agreement with similar measurements (132.5 - 180.0 nm) on the $N_2(a^1\Pi_g - x^1\Sigma_g^+)$ Lyman-Birge-Hopfield band system in the range of overlap (132.5 - 165.0 nm).

In this work a calibration curve of the relative sensitivity was established from 106.0 nm to 165.0 nm using the Lyman band system. Results were analyzed using the most intense band ($v'=3$, $v''=4$) which was normalized to 1. Using band heights of an unresolved rotational spectrum (see Fig. 10) and band transition probabilities (see Table 6), a relative intensity plot such as that shown in Fig. 6 was obtained. Similar results were obtained using photon counts integrated over one minute. In this case either the R(0) (see Table 7(a)) or P(2) branch (see Table 7(b)) of a band was counted and normalized to the respective transition of the $v'=3, v''=4$ band. The relative intensity is plotted in Fig. 6.

Similar calculations were carried out using data from twenty six spectra taken under a variety of conditions. The results shown in Fig. 6 are typical. The average scatter obtained was about 25% which is similar in magnitude to that obtained by other workers. This scatter is largely attributed to incomplete resolution.

The overall distribution of the relative sensitivity is consistent for individual measurements and conforms to the limits of sensitivity imposed by the LiF window material and the Channel Electron Multiplier sensitivity (see Fig. 5).

Table 6. Intensity calibration of relative sensitivity of the detecting system using 1st order low resolution Lyman Bands. Slit widths 500μ ; Total pressure 1.67×10^4 Pa; Lamp pressure 8.26×10^2 Pa; Hydrogen partial pressure $1.63 \times$ Pa; Spectrum was taken in first order from 110-165 nm at a scan rate of 0.1 nm/min.

Notes from Table:

- (a) Values taken from Ref.55.
- (b) Wavelength was recorded at centre of observed band.

TABLE 6
1st order calibration data

Wavelength λ (nm)	Transition (v', v'')	Einstein transition probability $A_{v'v''}$ ($\times 10^{-8} \text{ s}^{-1}$)	$A(3,4)_2$ $\frac{A(v', v'')_1}{A(v', v'')_2}$	Detector response $S(\lambda_{v'}, v'')$	$S(\lambda_{v'}, v'')_1$ $\frac{S(\lambda_{v'}, v'')_1}{S(\lambda_{v'}, v'')_2}$	Relative sensitivity $k(\lambda_{v'}, v'')_1$ $\frac{k(\lambda_{v'}, v'')_1}{k(\lambda_{3,4})_2}$
112.1	(3,1)	2.278	0.726	0	0	0
116.8	(3,2)	0.880	1.878	6.7	0.0981	0.1842
127.4	(3,4)	1.653	1.000	68.3	1.0000	1.0000
133.3	(3,5)	0.659	2.509	16.3	0.2387	0.5989
138.8	(3,6)	0.309	5.343	2.5	0.0366	0.1955
144.5	(3,7)	1.806	0.915	7.7	0.1127	0.1032
149.2	(3,8)	0.328	5.040	0.8	0.0117	0.0590
154.0	(3,9)	1.104	1.497	1.0	0.0146	0.0219
159.9	(3,10)	3.469	0.477	3.6	0.0527	0.0251
163.9	(3,11)	1.497	1.104	1.8	0.0264	0.0291

Table 7. Intensity calibration of relative sensitivity of the detecting system using high resolution Lyman bands.
Slit widths 150μ ; Total pressure 9.25×10^2 Pa; Hydrogen partial pressure 2.29×10^2 Pa; Lamp pressure 3.54×10^2 ;
Counting rates taken in 4th order.

- (a) Signals normalized to R(0) branch of (3,4) transition.
- (b) Normalized to P(2) branch of (3,4) transition.

Notes from Table:

- (a) Values taken from Ref.58.

TABLE 7 (a)
4th order calibration data

Wavelength (b) $\lambda(\text{nm})$	Transition (v', v'')	Einstein transition probability (a) $A_{v', v''}$ ($\times 10^{-8} \text{ s}^{-1}$)	$A(3,4)_2$ $\frac{A(v', v'')_1}{A(v', v'')_2}$	Detector response $S(\lambda_{v', v''})$	$S(\lambda_{v', v''})_1$ $\frac{S(\lambda_{v', v''})_1}{S(\lambda_{v', v''})_2}$	Relative sensitivity $k(\lambda_{v', v''})_1$ $\frac{k(\lambda_{v', v''})_1}{k(\lambda_{3,4})_2}$
106.28	(3,0)	0.336	1.625	21	0.013	0.021
111.20	(3,1)	0.759	0.719	29	0.018	0.013
116.27	(3,2)	0.305	1.790	396	0.247	0.442
126.84	(3,4)	0.546	1.000	1604	1.000	1.000
132.28	(3,5)	0.232	2.350	513	0.320	0.752
137.77	(3,6)	0.093	5.870	95	0.059	0.348
143.26	(3,7)	0.600	0.910	275	0.171	0.156
148.68	(3,8)	0.132	4.140	23	0.014	0.059
153.93	(3,9)	0.325	1.680	16	0.010	0.017
158.86	(3,10)	1.187	0.460	32	0.020	0.010

TABLE 7. (b)
4th order calibration data

Wavelength λ (nm)	Transition (v', v'')	Einstein transition probability $A_{v'v''}$ ($\times 10^{-8} \text{ s}^{-1}$)	$A(3,4)_2$ $\frac{A(v', v'')}{A(v', v'')_1}$	Detector response $S(\lambda_{v', v''})$	$S(\lambda_{v', v''})_1$ $\frac{S(\lambda_{v', v''})}{S(\lambda_{v', v''})_1}$	Relative sensitivity, $k(\lambda_{v', v''})_1$ $\frac{k(\lambda_{v', v''})}{k(\lambda_{v', v''})_1}$
106.68	(3,0)	0.705	1.57	40	0.025	0.0403
111.62	(3,1)	1.518	0.731	131	0.084	0.0615
116.71	(3,2)	0.555	2.00	314	0.201	0.4030
127.30	(3,4)	1.110	1.00	1558	1.000	1.000
132.75	(3,5)	0.401	2.77	388	0.249	0.6898
138.25	(3,6)	0.240	4.63	93	0.059	0.2764
143.74	(3,7)	1.205	0.921	173	0.111	0.1023
149.16	(3,8)	0.196	5.66	19	0.012	0.0690
154.39	(3,9)	0.779	1.42	23	0.014	0.0210
159.33	(3,10)	2.382	0.466	26	0.016	0.0078

REFERENCES

1. D. L. Baulch, D. D. Drysdale, ~~D. G.~~ Horne and A. C. Lloyd. Evaluated kinetic data for high temperature reactions. Butterworths, London. Vol. 2, 1972. p. 171.
2. M. A. Clyne and H. W. Cruse. J. Chem. Soc. Far. Trans. II. 68, 1281 (1972).
3. P. Warneck. J. Opt. Soc. Am. 55, 921 (1965).
4. P. G. Wilkinson and E. T. Byram. Appl. Optics. 4, 581 (1965).
5. P. P. Bemand and M. A. Clyne. J. Chem. Soc. Far. Trans. II. 69, 1643 (1973).
6. C. H. Petley. Channel electron multipliers, Mullard Industrial Electronics Division Bulletin UDC 621.383.81.
7. R. C. Weast. ed. Handbook of chemistry and physics 54th edition. CRC Press. 1974.
8. G.M. Provencher. PhD. Thesis, University of Windsor, Windsor, Ontario. 1972.
9. M. A. Clyne and B. A. Thrush, Proc. Roy. Soc. A. 261, 259 (1961).
10. R. F. Heidner III and J. V. Kasper. Chemical Physics Letters 15, 179 (1972).
11. J. H. Birely, J. V. Kasper, F. Hai and L. A. Darnton, Chem. Phys. Lett. 31, 22 (1975).
12. D. H. Stedman, D. Steffenson and H. Niki, Chem. Phys. Lett. 7, 173 (1970).
13. J. C. Polanyi and C. M. Sadowski. J. Chem. Phys. 36, 2239 (1962).
14. J. H. Birely and J. L. Lyman, J. Photochemistry 4, 269 (1975).
15. J. Ross, J. C. Light and K. E. Schuler, in A. R. Hochstim (ed.) Kinetic processes in gases and plasmas. Academic Press, New York. 1969. p. 281.
16. J. K. Kinsey. J. Chem. Phys. 54, 1206 (1971).
17. R. D. Levine and R. B. Bernstein. Acc. Chem. Res. 7, 393 (1974).

18. J. C. Polanyi. Faraday Discuss. Chem. Soc. 55, 389 (1973).
19. E. R. Fisher. Plumechemistry models. Summary of a plume chemistry workshop. AFCRL-TR-73-0697, ARPA No. 1E40. Advanced Research Projects Agency. Arlington, Va. April 1973.
20. P. Crutzen. Can. J. Chem. 52, 1569 (1971).
21. R. Dubinsky and D. McKenney. Can. J. Chem. 53, 3531 (1975).
22. R. F. Heidner III. PhD. Thesis, University of California, Los Angeles. 1972.
23. J. H. Birely, J. V. Kasper, F. Hai and L. A. Darnton. A computer analysis of the reaction of vibrationally-excited hydrogen with atomic oxygen in a flowing afterglow experiment. Bulletin TR-0075(5270-20)-3, The Aerospace Corporation. 1974.
24. G. N. Lewis and M. Randall. Thermodynamics, McGraw Hill, New York. 1961.
25. R. W. Wood. Phil. Mag. 12, 499 (1906).
26. G. Herzberg and L. L. Howe. Can. J. Phys. 37, 636 (1959).
27. S. Takezawa, F. R. Innes, and Y. Tanaka. J. Chem. Phys. 46, 4555 (1967).
28. S. Takezawa, F. R. Innes, and Y. Tanaka. J. Chem. Phys. 45, 2000 (1966).
29. H. Beutler. Z. Physik. Chem. B27, 287 (1934).
30. H. Beutler. Z. Physik. 50, 581 (1928).
31. J. R. McNeely, G. S. Hurst, E. B. Wagner, and M. G. Payne. J. Chem. Phys. 63, 2717 (1975).
32. C.K.N. Patel. Lasers, Vol. 2. Arnold, London. 1968.
33. E. H. Fink, D. Wallach, and C. B. Moore. J. Chem. Phys. 56, 3608 (1972).
34. G. Piper, J. E. Velazco, and D. W. Setser. J. Chem. Phys. 59, 3323 (1973).
35. D. H. Stedman and D. W. Setser. Prog. React. Kin. 6, 4 (1971).

36. J. A. Coxon, D. W. Setser and W. H. Duewer. J. Chem. Phys. 77, 124 (1973).
37. G. W. Taylor. J. Phys. Chem. 77, 124 (1973).
38. D. W. Setser, D. H. Stedman, and J. A. Coxon. J. Chem. Phys. 53, 1004 (1970).
39. D. H. Stedman and D. W. Setser. J. Chem. Phys. 52, 3957 (1970).
40. E. H. Fink, D. A. Atkins, and C. B. Moore. J. Chem. Phys. 56, 900 (1972).
41. N. Thonnard and G. S. Hurst. Phys. Rev. A5, 768 (1964).
42. H. A. Koehler. Phys. Rev. A9, 768 (1974).
43. W. Kolos and L. Wolniewicz. J. Chem. Phys. 41, 3663 (1964); 43, 2429 (1965); 45, 509 (1966); 48, 3672 (1968); 49, 404 (1968); Phys. Rev. Lett. 20, 243 (1968).
44. L. Wolniewicz. J. Chem. Phys. 45, 515 (1966).
45. P. G. Wilkinson. Can. J. Phys. 46, 1228 (1968).
46. T. Lyman. Astrophys. J. 33, 98 (1911).
47. E. E. Witmer. Phys. Rev. 28, 1223 (1926).
48. G. H. Dieke and J. J. Hopfield. Phys. Rev. 30, 400 (1927).
49. K. Mie. Z. Physik. 91, 475 (1934).
50. A. C. Mitchell and M. W. Zemansky. Resonance radiation and excited atoms. Cambridge University Press, American Branch, New York. 1971. p. 56.
51. H. Kallman and F. London. Z. Physik. Chem. B2, 207 (1929).
52. W. F. Mott and H. S. W. Massey. The theory of atomic collisions. Clarendon Press, Oxford, England. 1965. p. 650.
53. G. M. Burnett and A. M. North. Transfer and Storage of energy by molecules, Vol. I. Wiley-Interscience, London. 1969. p.21.
54. J. E. Hesser. J. Chem. Phys. 48, 2518 (1968).
55. A. C. Allison and A. Dalgarno. At. Data. 1, 289, (1970).

56. J. W. McConkey. J. Op. Soc. Am. 59, 110 (1969).
57. O. Stern and M. Volmer. Phys. Zeits. 201, 183 (1919).
58. K. H. Becker, E. H. Fink, and A. C. Allison. J. Op. Soc. Am. 61, 495 (1971).
59. M. Clyne and D. H. Stedman. Trans. Faraday Soc. 62, 2164 (1966).
60. M. Dunn, M. Sutton, C. Freeman, M. McEwan, and L. Phillips. J. Phys. Chem. 75, 722 (1971).
61. K. Mie. Z. Physik. 91, 475 (1934).
62. E. C. Kemble and V. Guillemin. Proc. Natl. Acad. Sci. U.S. 14, 728 (1928); H. H. Hyman. Phys. Rev. 36, 187 (1930).
63. R. G. Gordon. J. Chem. Phys. 44, 3083 (1966).
64. C. H. Townes and A. L. Schawlow. Microwave Spectroscopy. McGraw-Hill, New York. 1965.
65. Y. Tanaka, A. S. Jursa, and F. J. LeBlanc. J. Opt. Soc. Am. 45, 710 (1955); 48, 304 (1958).
66. R. G. Newburgh, L. Heroux, H. E. Hinteregger. Appl. Opt. 1, 733 (1962).
67. R. E. Huffman, Y. Tanaka, and J. C. Larrabee. Appl. Opt. 2, 617 (1963).
68. P. G. Wilkinson and E. T. Byram. Appl. Opt. 4, 581 (1965).
69. A. J. Gordon and A. F. Richard. The chemists companion. John Wiley and Sons, Toronto. 1972. p. 410.
70. F. Roseburg. Handbook of electron tube and vacuum techniques. Addison Wesley Publishing Company, Reading, Mass. 1965. p. 105.
71. J. A. R. Samson. Techniques of vacuum ultraviolet spectroscopy. John-Wiley and Sons, Inc., New York. 1967.
72. E. Shreider. Soviet Physics - Technical Physics. 9, 1609 (1965).
73. J. F. M. Aarts and F. J. de Heer, J. Opt. Soc. Am. 58, 1666 (1968).

74. M. J. Mumma and E. C. Zipf. J. Opt. Soc. Am. 61, 83 (1971).
75. D. E. Shemansky. J. Chem. Phys. 51, 5487 (1969).
76. W. L. Fite and R. T. Brackman. Phys. Rev. 112, 1151 (1958).
77. G. M. Lawrence. Phys. Rev. A2, 397 (1970).
78. G. Herzberg, Molecular spectra and molecular structure I. Spectra of diatomic molecules. Van Nostrand Reinhold, New York. 1950.

VITA AUCTORIS

Born:

August 28, 1951 at Windsor, Ontario, Canada.
Son of Mrs. Stella Pali and the late Mr.
Nicholas Dubinsky.

Primary Schools:

John C. Campbell, Windsor, Ontario.

General Brock, Windsor, Ontario.

Secondary School:

J. L. Forster Collegiate Ins., Windsor, Ontario.

Post Secondary School:

University of Windsor, Windsor, Ontario.
1974 - Bachelor of Science (Honours Chemistry).
1974 - Entered Faculty of Graduate Studies.

Awards:

1971-1972 Windsor Rotary Club Bursary.

1973-1974 President's Roll of Scholars -
University of Windsor.

Offices Held:

1974 - Chairman, Sandwich Festival Committee.
- Graduate Representative, Chemistry
Departmental Council.
- President, Chemistry Club.

1975 - President, Science Club.
- Editor, Science Club Newsletter.
- Chairman, Students' Administrative Council
Clubs Financial Appeal Board.

1976 - Executive Board, Windsor Canada Week
Committee.

Professional Affiliations:

The Chemical Institute of Canada

Publications:

R. Dubinsky and D. J. McKenney. Can. J. Chem. 53,
3551 (1975).